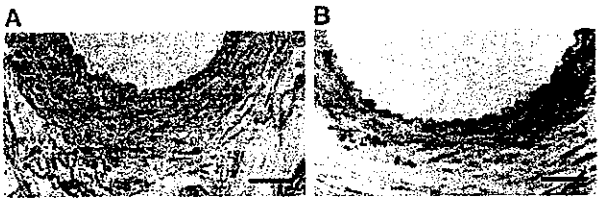

Figure 5. Sections of the femoral arteries harvested 14 days after the induction of injury stained with hematoxylin and eosin. Cross section of the femoral arteries from OPN-Tg (A) and non-Tg (B) mice. Intima is shown within the internal elastic lamina. OPN-Tg mice show more neointimal formation in response to cuff injury than non-Tg mice. Bar=20 μm.

shows representative cross sections of femoral arteries harvested 14 days after the induction of injury. The intima appears within the internal elastic lamina. More neointima forms in response to cuff injury in OPN-Tg than in non-Tg mice. Although inflammatory cells are located within the adventitia of both non-Tg and OPN-Tg mice, very little neointima forms in non-Tg. The morphometric measurements of the intimal and medial thickness 14 days after injury in both groups of mice are shown in the Table. No control intima was present in the femoral arteries of either OPN-Tg or non-Tg mice, and the control medial thickness in OPN-Tg mice was larger than that in non-Tg mice like aorta. The extent of the cuffed intimal thickening in OPN-Tg mice increased 2.9-fold more than that in non-Tg mice (4.9±1.9 versus 1.7±0.4 μm; $P=0.022$). The overexpression of OPN was also associated with a 1.3-fold increase in cuffed medial thickening in comparison to the medial thickening observed in non-Tg mice (16.1±2.7 versus 12.7±1.8 μm; $P=0.046$). Because the cuffed medial thickness increased less than the cuffed intimal thickness, the intima/media ratio was much higher in OPN-Tg (26.1±9.6%), than in non-Tg (12.9±3.5%; $P=0.034$) mice.

Zymography

We performed zymography to confirm whether MMP-2 and MMP-9 was expressed in the aorta of either OPN-Tg or non-Tg. The amount of active MMP-2 increased by 6.1±1.9-fold ($P<0.01$) in the aortas from OPN-Tg mice compared with those from non-Tg mice, and the pro–MMP-2 also differed (1.6±0.4-fold; $P<0.05$) (Figure 6). Pro–MMP-9 also increased in the aortas from OPN-Tg mice (3.3±0.4-fold; $P<0.0001$). These findings indicate that OPN might stimulate MMP-2 and MMP-9 production.

Response to Vessel Injury in OPN-Tg and Non-Tg Mice

	OPN-Tg	Non-Tg	*P*
No.	5	5	...
Control intima, μm	0	0	...
Control media, μm	15.5±1.7	13.5±1.3	0.05
Cuffed intima, μm	4.9±1.9	1.7±1.9	0.022
Cuffed media, μm	16.5±2.7	12.7±1.8	0.046
Cuffed I/M ratio, %	26.1±9.6	12.9±3.5	0.034

I/M ratio indicates intima/media ratio ($\mu m^2/\mu m^2 \times 100$).
Values represent the mean±SD.

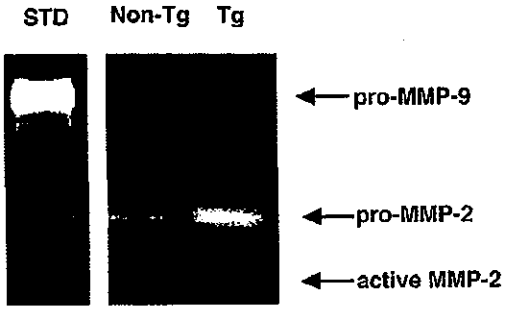

Figure 6. Representative gelatin zymographic analysis of protein extracts from the aortas of OPN-Tg and non-Tg. Active MMP-2 and pro–MMP-9 were more prevalent in OPN-Tg. Purified MMP-2 and MMP-9 protein were used standard (STD) in zymography (left lane).

SMC Migration

To assess the ex vivo effects of OPN on SMC migration in the OPN-Tg, we examined the ability of SMCs to migrate out from aortic explants. Explant migration of aortic SMCs was performed with OPN-Tg or non-Tg. After 8 days from the aortic explant, a 16- to 27-fold promotion of migration compared with non-Tg was observed in the OPN-Tg (Figure 7). This result correlates with the findings obtained in the cuff model and suggest that OPN strongly contributes to the promotion of SMC migration.

Discussion

The present study shows that high levels of OPN are expressed in the medial layer of the aorta in OPN-Tg mice and that medial thickening in these animals increased from 73% to 94% more than that in non-Tg mice. This study also shows that more neointima formed after arterial injury in OPN-Tg than in non-Tg mice. These results suggest that OPN plays an important role in the pathological processes associated with arterial SMC proliferation, such as atherosclerosis and restenosis.

The present study demonstrates that the level of OPN expression significantly increased in the SMCs of OPN-Tg mice and that medial thickening increased significantly more in OPN-Tg than in non-Tg mice. Furthermore PCNA staining showed evidence of cell proliferation in the SMCs of the media of OPN-Tg mice. These findings suggest OPN expression to be associated with SMC proliferation. Recent reports show that OPN is upregulated in the aortas of mice with

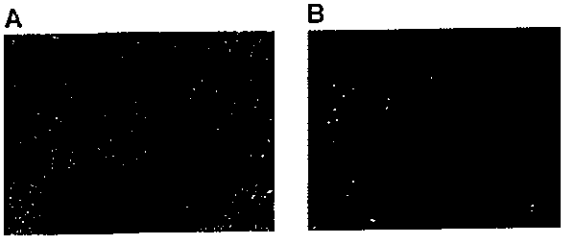

Figure 7. Explants of the aortas. SMCs started to grow out from the explants after 5 to 10 days in culture. At 8 days after explant, the SMC number increased more in OPN-Tg (A) than in non-Tg (B). Bar=200 μm.

diabetes induced by a high-fat diet[22] and in the forearm arteries of patients with diabetes mellitus.[23] These reports suggest that OPN production in vascular SMCs synergically augment their migration and proliferation and, thereby, facilitate the development of atherosclerosis in diabetes mellitus. The suggestions of our and other's studies are supported by the results of other in vitro studies. Giachelli et al[9] reported the OPN mRNA level to be higher in cultured pup cells, which have a high proliferative capacity, than in adult SMCs. Gadeau et al[13] analyzed the OPN expression in serum-stimulated quiescent SMCs and in asynchronously cycling SMCs in vitro and demonstrated that OPN overexpression is associated with SMC proliferation. These results suggest that an OPN expression is closely related to arterial SMC proliferation both in vitro and in vivo.

Regarding the factors of medial thickening, there are several ones, such as hemodynamic factors and inflammation. Blood pressure-induced stretch provokes remodeling in vascular SMCs[24] and transmural pressure promotes SMC proliferation.[25] However, no such hemodynamic effects significantly affected the medial layer thickening induced by OPN overexpression, because a pressure study revealed that the systolic blood pressure of OPN-Tg mice was as low as that of non-Tg mice. We therefore believe that the medial thickening in OPN-Tg mice was not due to hemodynamic factors. Although the adhesion of mononuclear cells to, and their infiltration into, the blood vessel wall is associated with the induction of medial thickening,[26–28] we also believe that inflammation is not responsible for the medial thickening observed in our Tg mice. Because the analysis of hematoxylin and eosin–stained sections (Figures 2A and 2B) showed no evidence of inflammatory cells adhering to endothelial cells or their infiltration into the vessel wall in any region in the OPN-Tg mice.

Our analysis of zymography confirmed that MMP-2 or MMP-9 did increase in the OPN-Tg aorta, but they were not expressed to a significant degree in the normal mouse aorta. This result is partly supported by the results of a previous in vitro study in which the stimulation of SMCs with OPN was reported to increase matrix metalloproteinases.[29] Furthermore, another in vitro study showed that OPN-stimulated MMP-2 activation occurred through NF-κB–mediated induction of membrane type 1 MMP, and thus, that report suggested that OPN-induced MMP-2 production could be regulated at the transcriptional level.[30] The increase in the amount of MMP-2 and MMP-9 in the OPN-Tg may thus play an important role in the destruction of the elastic lamina and the promotion of the explant migration of aortic SMCs.

OPN promotes rat and bovine SMC migration.[31] High levels of OPN mRNA and protein are detectable in the rat and human aorta and carotid arteries during neointima formation.[10,11,32,33] Moreover, Panda et al[14] suggested that the migration of SMCs from their original location in the arterial media toward the intima may be closely related to high circulating levels of OPN in the blood. However, there was no neointimal formation in our OPN-Tg mice without cuff-induced injury, although the levels of both OPN mRNA and serum OPN protein in OPN-Tg mice were high and immunohistochemistry revealed that SMCs of the aorta derived from OPN-Tg mice were positive for the anti-mouse OPN antibody. Furthermore, the explant migration of aortic SMCs increased in OPN-Tg mice. These results suggest that SMC migration and neointima formation by OPN are induced when the intima is impaired. Indeed, most in vivo studies, which suggest that OPN may play a role in SMC migration and/or neointima formation, were performed under such conditions, namely atherosclerosis[10,11,32] and after angioplasty.[14]

The migration of SMCs to the site of injury caused by angioplasty and a subsequent proliferation suggest the mechanisms of restenosis.[34–36] OPN mRNA is expressed in the both rat aorta and carotid arteries, and the expression levels are significantly elevated after balloon angioplasty, thus suggesting an important role for this matrix protein in vascular remodeling.[9] Our results indicate that OPN overexpression increases the neointimal proliferative response to vessel injury from cuff placement. Taken together, these data imply that OPN plays a role in the development of restenosis after angioplasty and these findings also lead us to assume that the inhibition of OPN gene expression at sites of injury may thus be viewed as a new therapeutic approach for preventing restenosis. Indeed, previous studies have demonstrated that a blockade of $\alpha_v\beta_3$ integrin, an OPN receptor and mediator of SMC migration after angioplasty,[15,28] resulted in a reduction of neointimal formation.[14] Furthermore, another recent study reported that neutralizing antibodies against OPN decreased the neointimal areas and cell numbers after endothelial denuation.[12]

In conclusion, this study demonstrated that OPN plays an important role in the development of vascular medial thickening without injury and in neointima formation after arterial injury in vivo.

Acknowledgments

These studies were supported in part by New Energy and Industrial Technology Development Organization (NEDO) Grants.

References

1. Miyauchi A, Alvarez J, Greenfield EM, Teti A, Grano M, Colucci S, Zambonin-Zallone A, Ross FP, Teitelbaum SL, Cheresh DA, Hruska KA. Recognition of osteopontin and related peptides by an $\alpha_v\beta_3$ integrin stimulates immediate cell signals in osteoclasts. *J Biol Chem.* 1991;266: 20369–20374.
2. Oldberg A, Franzen A, Heinegard D. Cloning and sequence analysis of rat bone sialoprotein (osteopontin) cDNA reveals an Arg-Gly-Asp cell-binding sequence. *Proc Natl Acad Sci U S A.* 1986;83:8819–8823.
3. Butler WT. Structural and functional domains of osteopontin. *Ann N Y Acad Sci.* 1995;760:6–11.
4. Reinholt FP, Hultenby K, Oldberg A, Heinegard D. Osteopontin: a possible anchor of osteoclasts to bone. *Proc Natl Acad Sci U S A.* 1990; 87:4473–4475.
5. Weber GF, Ashkar S, Glimcher MJ, Cantor H. Receptor-ligand interaction between CD44 and osteopontin (Eta-1). *Science.* 1996;271: 509–512.
6. Brown LF, Berse B, van de Water L, Papadopoulos-Sergiou A, Perruzzi CA, Manseau EJ, Dvorak HF, Senger DR. Expression and distribution of osteopontin in human tissues: widespread association with luminal epithelial surfaces. *Mol Biol Cell.* 1992;3:1169–1180.
7. Miyazaki Y, Setoguchi M, Yoshida S, Higuchi Y, Akizuki S, Yamamoto S. The mouse osteopontin gene: Expression in monocytic lineages and complete nucleotide sequence. *J Biol Chem.* 1990;265:14432–14438.
8. Patarca R, Freeman GJ, Singh RP, Wei FY, Durfee T, Blattner F, Regnier DC, Kozak CA, Mock BA, Morse HC III , Jerrells TR, Cantor H. Structural and functional studies of the early T lymphocyte activation 1 (Eta-1) gene: definition of a novel T cell–dependent response associated

with genetic resistance to bacterial infection. *J Exp Med.* 1989;170: 145–161.
9. Giachelli C, Bae N, Lombardi D, Majesky M, Schwartz S. Molecular cloning and characterization of 2B7, a rat mRNA which distinguishes smooth muscle cell phenotypes in vitro and is identical to osteopontin (secreted phosphoprotein I, 2aR). *Biochem Biophys Res Commun.* 1991; 177:867–873.
10. Ikeda T, Shirasawa T, Esaki Y, Yoshiki S, Hirokawa K. Osteopontin mRNA is expressed by smooth muscle-derived foam cells in human atherosclerotic lesions of the aorta. *J Clin Invest.* 1993;92:2814–2820.
11. Giachelli CM, Bae N, Almeida M, Denhardt DT, Alpers CE, Schwartz SM. Osteopontin is elevated during neointima formation in rat arteries and is a novel component of human atherosclerotic plaques. *J Clin Invest.* 1993;92:1686–1696.
12. Liaw L, Lombardi DM, Almeida MM, Schwartz SM, Deblois D, Giachelli CM. Neutralizing antibodies directed against osteopontin inhibit rat carotid neointimal thickening after endothelial denudation. *Arterioscler Thromb. Vasc Biol.* 1997;17:188–193.
13. Gadeau AP, Campan M, Millet D, Candresse T, Desgranges C. Osteopontin overexpression is associated with arterial smooth muscle cell proliferation in vitro. *Arterioscler Thromb.* 1993;13:120–125.
14. Panda D, Kundu GC, Lee BI, Peri A, Fohl D, Chackalaparampil I, Mukherijee BB, Li XD, Mukherjee DC, Seides S, Rosenberg J, Stark K, Mukherjee AB. Potential roles of osteopontin and $\alpha_v\beta_3$ integrin in the development of coronary artery restenosis after angioplasty. *Proc Natl Acad Sci U S A.* 1997;94:9308 9313.
15. Liaw L, Lindner V, Schwartz SM, Chambers AF, Giachelli CM. Osteopontin and β_3 integrin are coordinately expressed in regenerating endothelium in vivo and stimulate Arg-Gly-Asp-dependent endothelial migration in vitro. *Circ Res.* 1995;77:665–672.
16. Kawarabayashi T, Shoji M, Sato M, Sasaki A, Ho L, Eckman CB, Prada CM, Younkin SG, Kobayashi T, Tada N, Matsubara E, Iizuka T, Harigaya Y, Kasai K, Hirai S. Accumulation of β-amyloid fibrils in pancreas of transgenic mice. *Neurobiol Aging.* 1996;17:215–222.
17. Isoda K, Kamezawa Y, Tada N, Sato M, Ohsuzu F. Myocardial hypertrophy in transgenic mice overexpressing human interleukin 1α. *J Card Fail.* 2001;7:355–364.
18. Craig AM, Smith JH, Denhardt DT. Osteopontin, a transformation-associated cell adhesion phosphoprotein, is induced by 12-O-tetradecanoyl-phorbol. *J Biol Chem.* 1989;264:9682–9689.
19. Fukuda T, Miki T, Yoshida T, Hatano M, Ohashi K, Hirosawa S, Tokuhisa T. The murine BCL6 gene is induced in activated lymphocytes as an immediate early gene. *Oncogene.* 1995;11:1657–1663.
20. Moroi M, Zhang L, Yasuda T, Virmani R, Gold HK, Fishman MC, Huang PL. Interaction of genetic deficiency of endothelial nitric oxide, gender, and pregnancy in vascular response to injury in mice. *J Clin Invest.* 1998;101:1225–1232.
21. Curci JA, Liao S, Huffman MD, Shapiro SD, Thompson RW. Expression and localization of macrophage elastase (matrix metalloproteinase-12) in abdominal aortic aneurysms. *J Clin Invest.* 1998;102:1900–1910.
22. Towler DA, Bidder M, Latifi T, Coleman T, Semenkovich CF. Diet-induced diabetes activates an osteogenic gene regulatory program in the aortas of low density lipoprotein-deficient mice. *J Biol Chem.* 1998;273: 30427–30434.
23. Takemoto M, Yokote K, Nishimura M, Shigematsu T, Hasegawa T, Kon S, Uede T, Matsumoto T, Saito Y, Mori S. Enhanced expression of osteopontin in human diabetic artery and analysis of its functional role in accelerated atherogenesis. *Arterioscler Thromb Vasc Biol.* 2000;20: 624 628.
24. Lehoux S, Tedgui A. Signal transduction of mechanical stresses in the vascular wall. *Hypertenston.* 1998;32:338–345.
25. Hishikawa K, Nakaki T, Marumo T, Hayashi M, Suzuki H, Kato R, Saruta T. Pressure promotes DNA synthesis in rat cultured vascular muscle cells. *J Clin Invest.* 1994;93:1975–1980.
26. Takemoto M, Egashira K, Usui M, Numaguchi K, Tomita H, Tsutsui H, Shimokawa H, Sueishi K, Takeshita A. Important role of tissue angiotensin-converting enzyme activity in the pathogenesis of coronary vascular and myocardial structural changes induced by long-term blockade of nitric oxide synthesis in rats. *J Clin Invest.* 1997;99:278–287.
27. Tomita H, Egashira K, Kubo-Inoue M, Usui M, Koyanagi M, Shimokawa H, Takeya M, Yoshimura T, Takeshita A. Inhibition of NO synthesis induces inflammatory changes and monocyte chemoattractant protein-1 expression in rat hearts and vessels. *Arterioscler Thromb Vasc Biol.* 1998;18:1456–1464.
28. Koyanagi M, Egashira K, Kitamoto S, Ni W, Shimokawa H, Takeya M, Yoshimura T, Takeshita A. Role of monocyte chemoattractant protein-1 in cardiovascular remodeling induced by chronic blockade of nitric oxide synthesis. *Circulation.* 2000;102:2243–2248.
29. Bendeck MP, Irvin C, Reidy M, Smith L, Mulholland D, Horton M, Giachelli Smooth muscle cell matrix metalloproteinase production is stimulated via $\alpha_v\beta_3$ integrin. *Arterioscler Thromb Vasc Biol.* 2000;20: 1467–1472.
30. Philip S, Bulbule A, Kundu GC. Osteopontin stimulates tumor growth and activation of promatrix metalloproteinase-2 through nuclear factor-κB–mediated induction of membrane type 1 matrix metalloproteinase in murine melanoma cells. *J Biol Chem.* 2001;276:44926–44935.
31. Liaw L, Almeida M, Hart CE, Schwartz SM, Giachelli CM. Osteopontin promotes vascular cell adhesion and spreading and is chemotactic for smooth muscle cells in vitro. *Circ Res.* 1994;74:214–224.
32. Shanahan CM, Cary NR, Metcalfe JC, Weissberg PL. High expression of genes for calcification-regulating proteins in human atherosclerotic plaques. *J Clin Invest.* 1994;93:2393–2402.
33. Liaw L, Skinner MP, Raines EW, Ross R, Cheresh DA, Schwartz SM, Giachelli CM. The adhesive and migratory effects of osteopontin are mediated via distinct cell surface integrins: role of $\alpha_v\beta_3$ in smooth muscle cell migration to osteopontin in vitro. *J Clin Invest.* 1995;95:713–724.
34. Ferrell M, Fuster V, Gold HK, Chesebro JH. A dilemma for the 1990s. Choosing appropriate experimental animal model for the prevention of restenosis. *Circulation.* 1992;85:1630–1631.
35. Austin GE, Ratliff NB, Hollman J, Tabei S, Phillips DF. Intimal proliferation of smooth muscle cells as an explanation for recurrent coronary artery stenosis after percutaneous transluminal coronary angioplasty. *J Am Coll Cardiol.* 1985;6:369–375.
36. Giraldo AA, Esposo OM, Meis JM. Intimal hyperplasia as a cause of restenosis after percutaneous transluminal coronary angioplasty. *Arch Pathol Lab Med.* 1985;109:173–175.

THE JOURNAL OF GENE MEDICINE
J Gene Med 2002; 4: 333–341.
Published online 9 May 2002 in Wiley InterScience (www.interscience.wiley.com). **DOI:** 10.1002/jgm.281

RESEARCH ARTICLE

High-level expression of naked DNA delivered to rat liver via tail vein injection

H. Maruyama[1]*
N. Higuchi[1]
Y. Nishikawa[2]
S. Kameda[1]
N. Iino[1]
J. J. Kazama[1]
N. Takahashi[1]
M. Sugawa[3]
H. Hanawa[4]
N. Tada[5]
J. Miyazaki[6]
F. Gejyo[1]

[1]*Division of Clinical Nephrology and Rheumatology, Niigata University Graduate School of Medical and Dental Sciences, 1-757 Asahimachi-dori, Niigata 951-8120, Japan*

[2]*Department of Pathology (I), Akita University School of Medicine, 1-1-1 Hondo, Akita 010-8543, Japan*

[3]*Pharmaceutical Technology Laboratory, Chugai Pharmaceutical Co., Ltd., 2-1-9 Kyobashi, Chuou-ku, Tokyo 104-8301, Japan*

[4]*Division of Cardiology, Niigata University Graduate School of Medical and Dental Sciences, 1-757 Asahimachi-dori, Niigata 951-8120, Japan*

[5]*Division of Biomedical Research Resources, Juntendo University School of Medicine, 2-1-1 Hongo, Bunkyo-ku, Tokyo 113-8421, Japan*

[6]*Division of Stem Cell Regulation Research, G6, Osaka University Medical School, 2-2 Yamadaoka, Suita 565-0871, Japan*

*Correspondence to: H. Maruyama, Division of Clinical Nephrology and Rheumatology, Niigata University Graduate School of Medical and Dental Sciences, 1-757 Asahimachi-dori, Niigata 951-8120, Japan.
E-mail: hirokim@med.niigata-u.ac.jp

Received: 18 January 2002
Revised: 11 March 2002
Accepted: 19 March 2002

Abstract

Background High levels of foreign gene expression in mouse hepatocytes can be achieved by rapid tail vein injection of a large volume of a naked DNA solution, the 'hydrodynamics-based procedure'. Rats are more tolerant of the frequent phlebotomies required for monitoring blood parameters than mice, and thus are better for some biomedical research.

Methods We tested this technique for the delivery of a therapeutic protein in normal rats, using a rat erythropoietin (Epo) expression plasmid vector, pCAGGS-Epo.

Results We obtained maximal Epo expression when the DNA solution was injected in a volume of 25 ml (approximately 100 ml/kg body weight) within 15 s. We observed a dose-response relationship between serum Epo levels and the amount of injected DNA up to 800 μg. Using quantitative real-time PCR, the vector-derived Epo mRNA expression was mainly detected in the liver. When a lacZ expression plasmid was injected similarly, β-galactosidase was exclusively detected in the liver, mainly in hepatocytes. Toxicity attributable to the technique was mild and transient, as assessed by histochemical analysis. Epo gene expression and erythropoiesis occurred with Epo gene transfer in a dose-dependent manner, and persisted for at least 12 weeks, the last time point examined. Repeated administration of the plasmid DNA also effectively led to erythropoiesis.

Conclusions These results demonstrate that gene transfer into the liver via rapid tail vein injection can easily be achieved in the rat, which is more than 10 times larger than the mouse, and has significant value for gene function analysis in rats. Copyright © 2002 John Wiley & Sons, Ltd.

Keywords naked DNA; rat; liver; erythropoietin; tail vein injection; hydrodynamics-based transfection

Introduction

The liver is an important target organ for gene transfer due to its large capacity for synthesizing serum proteins and its involvement in numerous genetic and acquired diseases. Thus, liver-targeted gene transfer is an important tool for expanding the treatment options for liver diseases and diseases affecting other organ systems, and for gene function studies. Among the various gene delivery systems available, naked DNA-mediated gene transfer is the simplest, and techniques for introducing naked DNA into hepatocytes have been the most intensely studied methods for generating therapeutic amounts of gene product. Hickman *et al.* [1] and Malone *et al.* [2] reported that the direct injection of naked DNA into the liver of both rats and cats can lead to significant levels of gene expression. Budker *et al.* [3] reported efficient gene expression in mouse hepatocytes following the

intraportal injection of naked DNA. Zhang *et al.* [4] reported unprecedented levels of reporter gene expression in hepatocytes following the direct injection of naked DNA into the liver vessels or bile ducts of mice, rats, and dogs. The major limitation of these methods is that they require local administration or surgical procedures. Recently, Liu *et al.* [5] and Zhang *et al.* [6] have developed a technique for expressing exogenous genes in mice, using the systemic administration of naked DNA. They found that extremely high levels of foreign gene expression in mouse hepatocytes can be achieved by the rapid injection of a large volume of a naked DNA solution into the tail vein [5]. However, in these reports, the reporter gene expression was transient, lasting only 1 week [5,6], probably because hepatocytes expressing foreign proteins are attacked by an immune response. Because of this, we believe that expressing a species-specific protein gene product would be more suitable for evaluating the utility of this technique. Compared with mice, rats are more tolerant of the frequent phlebotomy required for monitoring several blood parameters, and thus are more suitable subjects for several disease models. We found it difficult to perform the rapid injection of a large volume of a naked DNA solution into the rat tail vein using a syringe with an attached needle, because we could not achieve a secure needle placement. We therefore performed the tail vein injection using a syringe with a winged needle equipped with an external tube, which solved this problem. We chose the rat erythropoietin (Epo) gene for the present experiments, because its physiological effects can be easily monitored by performing serum Epo measurements and red blood cell (RBC) analyses of blood samples obtained from the treated rats, as previously described [7,8].

In the present study, we evaluated the effects of injection parameters on gene transfer efficiency, and the long-term effects of expressing the Epo gene in the rat liver by injecting pCAGGS-Epo, an Epo expression plasmid vector [7], via the tail vein.

Materials and methods

Plasmid DNA

We constructed plasmid pCAGGS-Epo [7] by inserting rat Epo cDNA into a unique *XhoI* site of the pCAGGS expression vector that has the CAG (cytomegalovirus immediate-early enhancer/chicken β-actin hybrid) promoter [9], and prepared the plasmid using a Qiagen EndoFree plasmid Giga kit (Qiagen GmbH, Hilden, Germany), as described previously [7]. We used the empty pCAGGS plasmid as a control.

Rats

Six-week-old male Wistar rats were purchased from Charles-River Japan Inc. (Tokyo, Japan). Two weeks later, we injected plasmid DNA into eight-week-old rats.

Plasmid DNA injection techniques

We diluted the plasmid DNA with Ringer's solution (Ohtsuka, Tokushima, Japan) at room temperature. We anesthetized the rats with diethyl ether. It is much harder to perform rapid tail vein injection in rats than in mice due to the thick skin that covers the rat tail vein and the fact that a higher injection pressure against vascular resistance is required. To cope with these problems, we used a SURFLO winged infusion set (Terumo, Tokyo, Japan) consisting of a 22-gauge winged needle 19-mm long and 0.7 mm in diameter, with an external tube 30-cm long and 1.1 mm in diameter (Figure 1). We injected various doses of plasmid DNA in various volumes of Ringer's solution through the winged needle connected to a 25-ml capacity syringe (Terumo), into the tail vein at various injection speeds. Hemostasis was seen at the injection site after applying pressure for 10 s.

Quantitative RT-PCR analysis

On the day after the injection, we sacrificed rats that had received 800 μg of pCAGGS-Epo, and harvested the liver. The total RNA of the liver sample was isolated by Isogen (Nippon Gene, Tokyo, Japan) and used for the synthesis of first-strand cDNA using Moloney murine leukemia virus reverse transcriptase (RT; Gibco BRL, Rockville, MD, USA) and random hexamers (Promega, Madison, WI, USA). The RT product was amplified by PCR with *Taq* DNA polymerase (Promega) and specific primers as follows: Epo backward primer, 5′-GCCCAGAGGAATCAG TAGCA-3′; Epo forward primer, 5′-TCTGACTGACCGCGT TACTC-3′; rat housekeeping gene, glucose-6-phosphate dehydrogenase (G6PDH) backward primer, 5′-TTCTTGG TCATCATCTTGGTGTAT-3′; G6PDH forward primer, 5′-TATCTCAGAGGTGGAAACTGACAA-3′. We designed the Epo forward primer to hybridize with the sequence

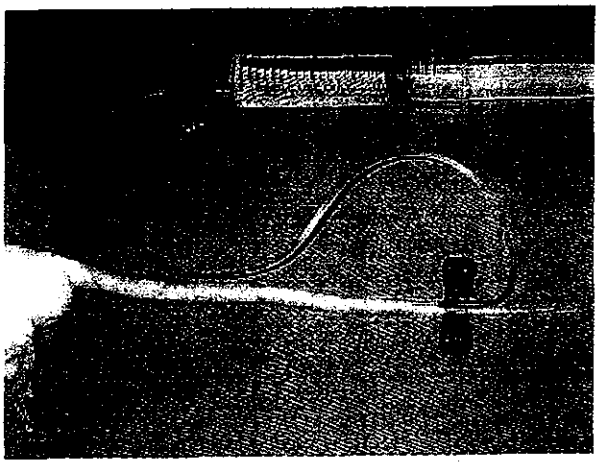

Figure 1. Rat tail vein injection through a SURFLO winged infusion set (Terumo), consisting of a 22-gauge winged needle 19-mm long and 0.7 mm in diameter, with an external tube 30-cm long and 1.1 mm in diameter, connected to a 25-ml capacity syringe

immediately downstream of the transcriptional start site of the CAG promoter. There is an intron between the CAG promoter and the Epo cDNA in pCAGGS-Epo. The primer set for the detection of the Epo mRNA encompasses an intron, allowing us to distinguish any possible PCR products from contaminating plasmid DNA or genomic DNA. The primer set for the detection of G6PDH mRNA was also designed to span introns. The lengths of the expected products were 170 bp for Epo mRNA and 342 bp for G6PDH mRNA. These PCR products were directly inserted into the pGEM-T Easy Vector (Promega), to create pGEM-T-Epo or pGEM-T-G6PDH, respectively. These plasmids were grown in *Escherichia coli* DH5α cells and prepared using a QIAprep Spin Miniprep kit (Qiagen) for use as the external standard.

To determine the levels of transgene-derived Epo mRNA in major organs, we performed quantitative real-time PCR analysis using a LightCycler Quick system 330 (Roche Diagnostics, Mannheim, Germany). The PCR was performed with LightCycler-FastStart DNA Master SYBR Green I (Roche Diagnostics), according to the manufacturer's protocol, and using the primer pairs described above. The PCR reaction consisted of 95°C for 10 min, then 95°C briefly, 62°C for 10 s, and 72°C for 13 s with a transition rate of 20°C/s between temperature plateaus, for a total of 40 cycles. The data were quantified using the LightCycler analysis software (version 3, Roche Diagnostic). A standard curve for the Epo plasmid was created, and the standard error was <0.001. The results were expressed initially as the number of target molecules/2 μl cDNA. To standardize the results for variability in RNA and cDNA quantity and quality, we quantified the total number of G6PDH transcripts in each sample as an internal control. Normalized levels of the Epo transcripts were calculated as the ratio of the number of Epo transcripts to G6PDH transcripts. We confirmed the RT-PCR products by 4% agarose gel electrophoresis.

Blood analyses

Serum rat Epo levels were determined as described [7]. The RBC, hematocrit, and reticulocytes were measured as described [8]. Serum concentrations of alkaline phosphatase (ALP), aspartate aminotransferase (AST), alanine aminotransferase (ALT), total bilirubin (TB), total protein (TP), albumin (Alb), lactate dehydrogenase (LDH), creatine phosphokinase (CPK), sodium (Na), potassium (K), and chloride (Cl) were measured by an Olympus AU 5200 automated analyzer (Olympus, Tokyo, Japan).

X-gal and immunohistochemical staining

pCAGGS-lacZ expresses *Escherichia coli* β-galactosidase [10]. We harvested the lung, heart, liver, spleen, and kidneys for X-gal staining 1 day after the injection of 800 μg of pCAGGS-lacZ, embedded them in Tissue-Tek O.C.T. compound (Sakura Finetechnical Co. Ltd., Tokyo, Japan), and froze them in a mixture of dry ice and acetone. We cut serial sections (5-μm thick) with a cryostat and placed them on glass slides coated with 3-aminopropyltriethoxysilane. We fixed the slices in 1.5% glutaraldehyde at room temperature for 10 min, then washed them three times in cold phosphate-buffered saline (PBS) (5 min/wash), and incubated them in an X-gal staining solution containing 1 mg/ml X-gal, 2 mM $MgCl_2$, 5 mM $K_4Fe(CN)_6$, 5 mM $K_3Fe(CN)_6$, and 0.5% Nonidet P-40 in PBS, pH 7.4, at 37°C for 3 h [11], followed by counterstaining with nuclear fast red.

Liver histology

We harvested the liver on days 1 and 7 after the naked DNA injection. The livers were fixed in 10% buffered formaldehyde, embedded in paraffin, and processed for routine light microscopy. We then stained 5-μm sections with hematoxylin and eosin (HE) for the detection of possible tissue injury due to the gene transfer procedure.

Statistical analysis

We have presented the data as the mean values ± the standard deviation of the mean. We analyzed all data using the StatView statistical program for Macintosh (SAS, Cary, NC, USA). We evaluated the statistical significance using the unpaired *t*-test. We considered *P* values of <0.05 to be statistically significant.

Results

Quantitative real-time PCR analysis for Epo mRNA in major organs

Because injecting plasmid DNA into the tail vein did not permit anatomical targeting of the DNA to the liver, it was important to examine whether the plasmid DNA was transfected into and expressed mainly in the liver and whether the expression of plasmid DNA was persistent. Normalized levels of the Epo transcripts were calculated as the ratio of Epo transcripts to G6PDH transcripts. We detected the transgene-derived Epo mRNA by quantitative real-time PCR in the liver, heart, lungs, and kidney of rats that had been injected with a 25-ml volume of 800 μg of pCAGGS-Epo (Figure 2). The control G6PDH mRNA was detected in all major organs. Among the organs examined, the level of Epo gene expression in the liver was the highest at each time point of the experiment. The ratio of Epo mRNA/G6PDH mRNA expression in the liver reached 15 on day 1, but rapidly dropped to 2 by week 1, and thereafter declined to 0.1 by week 12. Thus, the transgene expression by pCAGGS-Epo injected via the tail vein was seen on the first day after injection and was maintained for more than 12 weeks. The transgene expression in the heart, kidney, and lungs was much less (about 0.3%) than in the liver, but was also maintained for more than 12 weeks. The transgene-derived Epo mRNA was slightly detected in the spleen on day 1 after

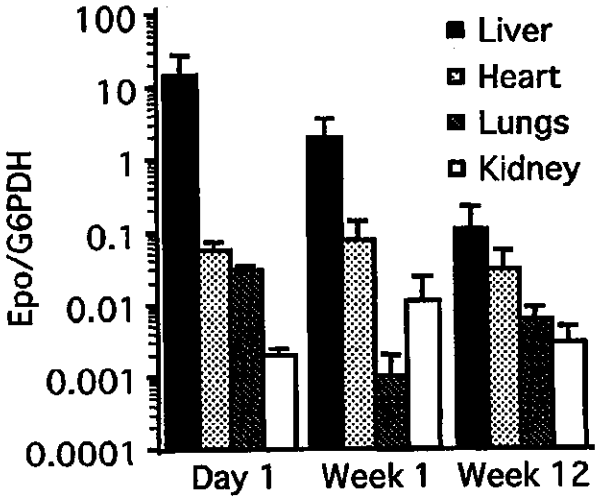

Figure 2. Tissue distribution of Epo mRNA expression 1 day, 1 week, and 12 weeks after pCAGGS-Epo injection. The levels of Epo mRNA and G6PDH in major organs were determined by real-time PCR analysis. Normalized levels of the Epo transcripts were calculated as the ratio of the number of Epo transcripts to the G6PDH transcripts. $n=3$ at each time point

injection (data not shown), but not detected at all in brain, muscle, skin, or testes.

Localization of pCAGGS-lacZ gene expression

To clarify the transgene expression site, we delivered 800 μg of pCAGGS-lacZ or pCAGGS into the tail vein. *LacZ* gene expression was assessed in various organs including the liver, heart, lungs, kidney, and spleen. X-gal stained only the liver of the pCAGGS-lacZ-injected rats (Figures 3a and 3b), but did not stain the liver of the pCAGGS-injected rats (data not shown). The stained cells were mainly hepatocytes, which were identifiable by their polygonal shape and round nuclei, visible at a higher magnification (Figure 3c). We did not find convincing examples of X-gal-stained cells in the heart, lungs, kidney, or spleen of the pCAGGS-lacZ-injected rats (data not shown).

Effects of injection parameters on gene transfer efficiency

In the following experiments, we used pCAGGS-Epo in a reporter assay, because we could easily monitor its physiological effects using serum Epo measurements and RBC analyses. Safety is of paramount importance in designing or evaluating a system for gene therapy. To obtain a 100% rat survival rate immediately after gene transfer, we first evaluated the injection volumes that caused death. Rats could not tolerate volumes larger than 25 ml (100 ml/kg body weight). Thus, in the subsequent study, we used injection volumes smaller than or equal to 25 ml. We evaluated the effects of varying the injection time (15–60 s) with a constant volume (25 ml), and

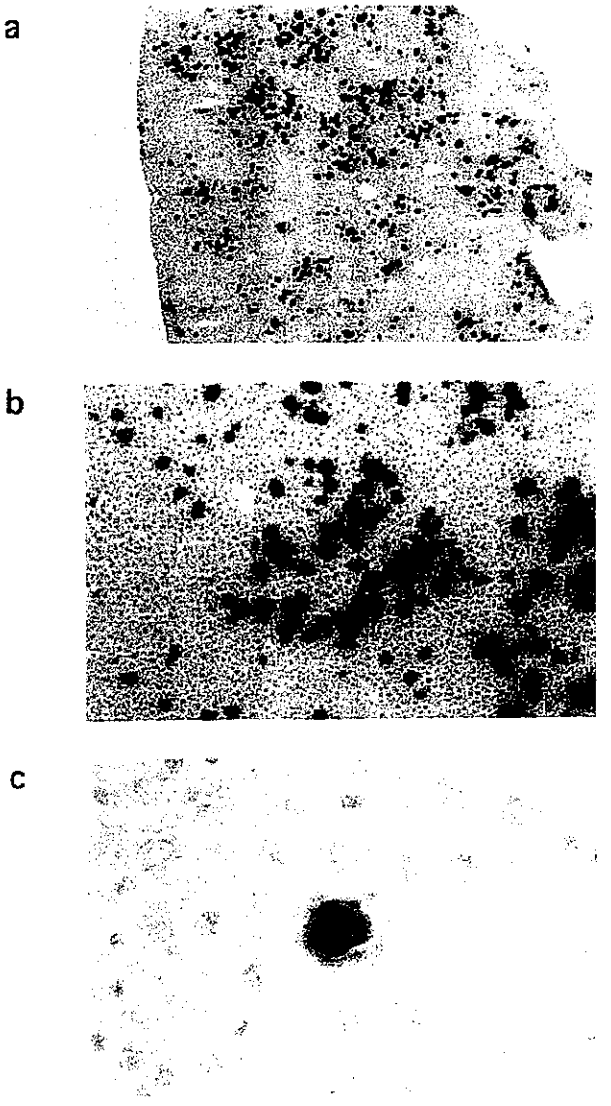

Figure 3. X-gal-stained rat liver section 1 day after injection with pCAGGS-lacZ. (a) Original magnification, ×30. (b) Original magnification, ×75. (c) Original magnification, ×600

varying the volume (5–25 ml) within a constant time (15 s) on the efficiency of gene transfer. We measured the serum Epo levels 1 week before and 1 week after injecting 800 μg of pCAGGS-Epo. As shown in Figures 4a and 4b, rapid injection and a large volume resulted in a higher level of transgene expression. We obtained maximal Epo expression when the DNA solution was injected within 15 s (Figure 4a) with a volume of 25 ml (Figure 4b). Injection volumes per kg body weight were 20.3 ± 0.7, 41.6 ± 1.2, 63.6 ± 4.2, 82.6 ± 1.5, and 102.1 ± 3.3 ml/kg for pCAGGS-Epo rats with injection volumes of 5, 10, 15, 20, and 25 ml, respectively. We next evaluated the effect of varying the amount of DNA injected in a <15-s injection time and a volume of 25 ml. We observed a dose-response relationship between serum Epo levels and the amount of injected DNA up to 800 μg, and substantial levels of Epo gene expression with only 10 μg of DNA (Figure 4c).

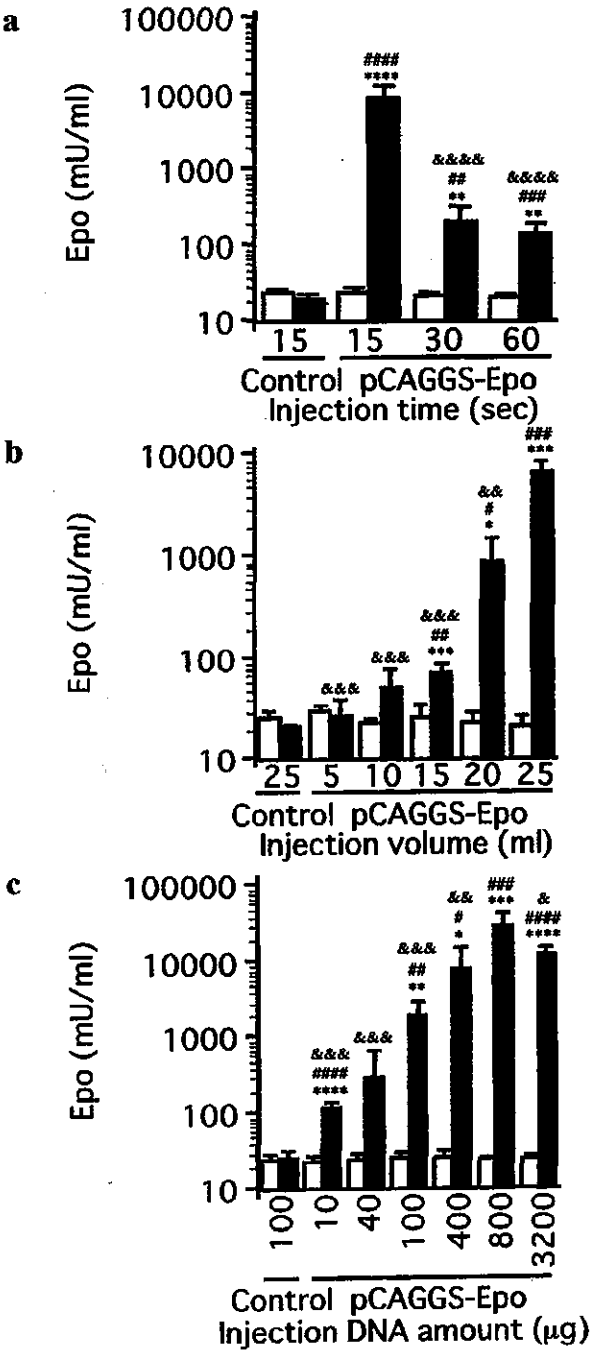

Figure 4. Effect of injection parameters on serum Epo levels. Serum Epo was measured 1 week before and 1 week after naked DNA injection. (a) Effect of injection time on serum Epo levels using 800 μg of pCAGGS-Epo or pCAGGS. $n=6$ in each group. (b) Effect of injection volume on serum Epo levels using 800 μg of pCAGGS-Epo or pCAGGS. $n=4$ in each group. (c) Effect of varying the amount of DNA injected on serum Epo levels. $n=6$ in each group. *, $P<0.05$; **, $P<0.01$; ***, $P<0.001$; and ****, $P<0.0001$ for comparisons with control rats (comparisons were made at each time point), #, $P<0.05$; ##, $P<0.01$; ###, $P<0.001$; and ####, $P<0.0001$ for differences between pre- and postinjection levels within each group. (a) &&&&, $P<0.0001$ for comparisons with the pCAGGS-Epo 15-s group. (b) &&, $P<0.01$ and &&&, $P<0.001$ for comparisons with the pCAGGS-Epo 25-ml group. (c) &, $P<0.05$; &&, $P<0.01$; and &&&, $P<0.001$ for comparisons with the pCAGGS-Epo 800-μg group

Time course of Epo expression after pCAGGS-Epo injection

We next evaluated the time course of the Epo expression after the injection of various amounts of DNA, using a <15-s injection time and a volume of 25 ml. Rats were assigned to five groups: each group was subjected to tail vein injection with either 800 μg of pCAGGS-Epo (pCAGGS-Epo 800 μg rats; $n=6$), 400 μg of pCAGGS-Epo (pCAGGS-Epo 400 μg rats; $n=6$), 100 μg of pCAGGS-Epo (pCAGGS-Epo 100 μg rats; $n=6$), 10 μg of pCAGGS-Epo (pCAGGS-Epo 10 μg rats; $n=5$), or 800 μg of pCAGGS (pCAGGS rats; $n=5$).

Compared with muscle-targeted Epo gene transfer [8], pCAGGS-Epo injection via the tail vein powerfully increased the serum Epo levels and induced polycythemia. Most of the rats injected with 400 μg or more of pCAGGS-Epo died of polycythemia after 12 weeks. The duration of the experiment, therefore, was limited by the loss of rats by death. The serum Epo levels in the control rats were not significantly increased. However, after injection with 800 μg of pCAGGS-Epo, the serum Epo levels peaked at 28 300±13 200 mU/ml at week 1, and gradually decreased to 820±630 mU/ml at week 12, which was the last time point examined. A similar pattern was obtained using smaller doses of plasmid (40, 100, or 400 μg of pCAGGS-Epo) until week 12, and 10 μg of pCAGGS-Epo until week 8. These data indicate that continuous delivery of Epo for more than 12 weeks can be achieved in rats by liver-targeted gene transfer via tail vein injection (Figure 5a). Transgene-derived Epo secretion caused reticulocytosis (Figure 5b). The hematocrit level was much higher in the rats injected with pCAGGS-Epo than in the pCAGGS-injected control rats, for at least 12 weeks, which was the last time point examined (Figure 5c). A dip in the hematocrit at week 8 was seen in each group. Epo gene transfer, therefore, could not explain this transient dip. Thus, pCAGGS-Epo transfer continuously produced biologically active Epo, resulting in a significant elevation of the reticulocyte and hematocrit levels in a dose-dependent manner.

Effect of readministration

The readministration of naked DNA is an important issue, because repeated therapy or dose escalation is required to treat many chronic diseases in humans. As shown in Figure 5a, 9 weeks after the first DNA injection we administered 40 ml of Ringer's solution (92.4±5.6 ml/kg) containing 100 μg of pCAGGS-Epo into rats previously injected with 10 μg of pCAGGS-Epo (pCAGGS-Epo10 μg: 100 μg rats). The other groups were left untreated. The serum Epo levels in the pCAGGS-Epo 10 μg rats peaked at 102.1±45.1 mU/ml 1 week after readministration, and gradually decreased to 44.1±15.6 mU/ml 3 weeks later. Subsequent reticulocytosis (Figure 5b) and increased hematocrit levels (Figure 5c) were also observed.

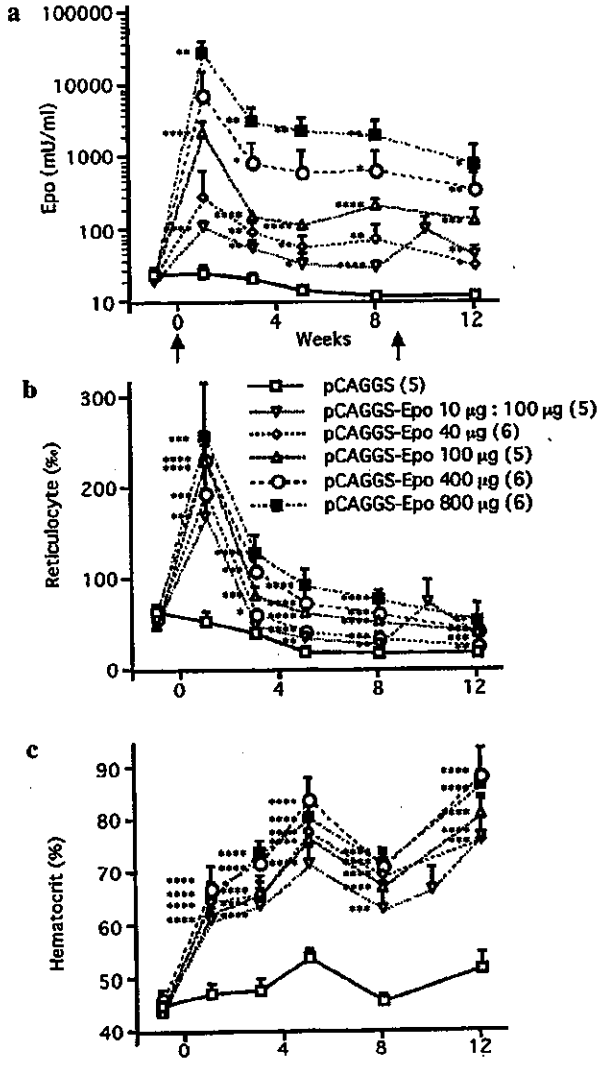

Figure 5. The time course after pCAGGS-Epo injection. Arrows at weeks 0 and 9 indicate the times of the first and second injections of the plasmid DNA. *, $P<0.05$; **, $P<0.01$; ***, $P<0.001$; and ****, $P<0.0001$, for comparisons between pCAGGS-Epo and control rats (comparisons were made at each time point). (a) Serum Epo levels. (b) Reticulocyte count. (c) Hematocrit. Error bars are not shown for some data points because of low variability

Toxicity evaluation after injection

To determine whether the procedure caused any adverse effects in the rats, we measured their serum chemistries. Rats were assigned to four groups: three groups were injected with 25 ml of Ringer's solution containing either 800 μg of pCAGGS-Epo (pCAGGS-Epo rats; $n=5$), 800 μg of pCAGGS (pCAGGS rats; $n=5$), or no DNA (Ringer's solution rats; $n=5$), and one group was not injected (control rats; $n=5$). All rats survived the injection. After the injection of Ringer's solution with or without plasmid DNA, the body weight remained elevated for 2 h, then slowly returned to baseline by 12 h. The serum ALT of the pCAGGS-Epo rats, pCAGGS rats, and Ringer's solution rats sharply increased on day 1 after the injection, returned to normal levels by day 3, and was maintained thereafter (Figure 6). Similarly, the serum AST of the pCAGGS-Epo rats, pCAGGS rats, and Ringer's solution rats abruptly increased on day 1 after the injection and returned to normal levels by day 3 (data not shown). The serum TP, Alb, ALP, TB, Na, K, and Cl of each group were within normal range at each time point (data not shown).

Histological examination for liver damage

To evaluate the likelihood of liver damage, we analyzed liver sections from rats injected with 25 ml of Ringer's solution containing either 800 μg of pCAGGS-Epo, 800 μg of pCAGGS, or no DNA, and compared them with liver sections from normal, uninjected rats. Compared with the uninjected rats (Figure 7a), no apparent pathological changes were observed in the liver sections of rats sacrificed on day 1 (Figure 7b) and day 7 after pCAGGS-Epo injection (Figure 7c). Similarly, no apparent pathological changes were observed in the liver sections of rats sacrificed on day 1 and day 7 after the pCAGGS, or no-DNA injections (data not shown).

Epo expression after pCAGGS-Epo injection in mice

Comparison with mouse tail vein injection is important to determine if the efficiency has really been optimized to match that in the mouse. Therefore, we have also assessed the efficiency of pCAGGS-Epo transfer by tail vein injection in mice. We need approximately 0.3 ml of blood for measurement of serum Epo levels. This level of phlebotomy lowers the hematocrit and stimulates endogenous Epo production in mice. Therefore, we obtained blood from each mouse only once. Six-week-old male ICR mice (25–29 g; Charles-River Japan Inc.) were assigned to

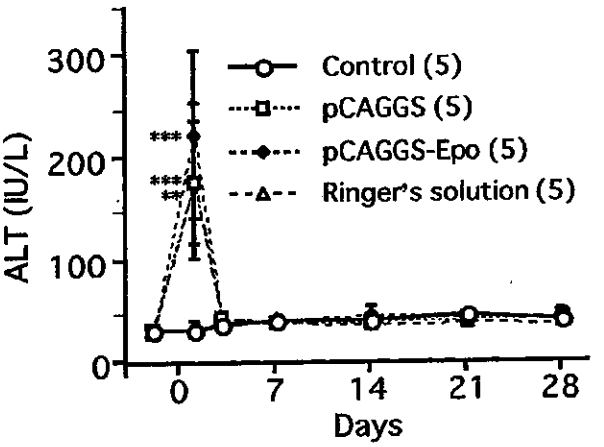

Figure 6. Effect of the tail vein injection technique on serum ALT. Rats were injected with pCAGGS, pCAGGS-Epo, or Ringer's solution. Control rats were not injected. $n=5$ in each group. **, $P<0.01$ and ***, $P<0.001$, for comparisons with normal rats (comparisons were made at each time point)

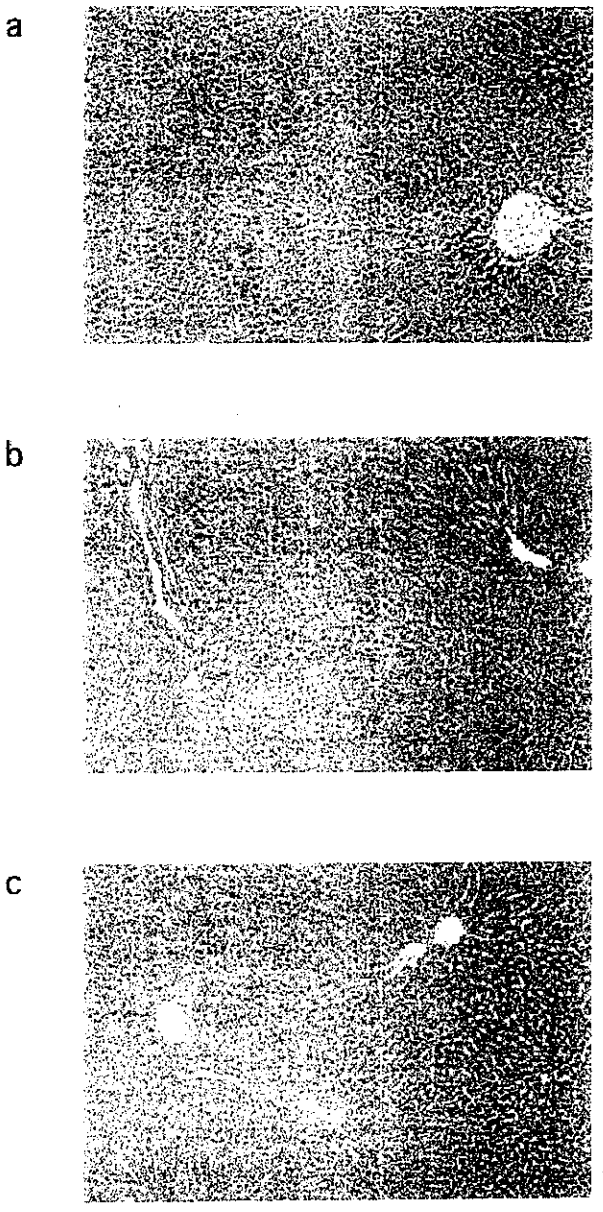

Figure 7. Histological examination for tissue damage by gene transfer. Liver sections were stained with HE. (a) Liver section of an uninjected rat. (b) Liver section 1 day after injection with 800 μg of pCAGGS-Epo. (c) Liver section 7 days after injection with 800 μg of pCAGGS-Epo. Original magnification, ×75

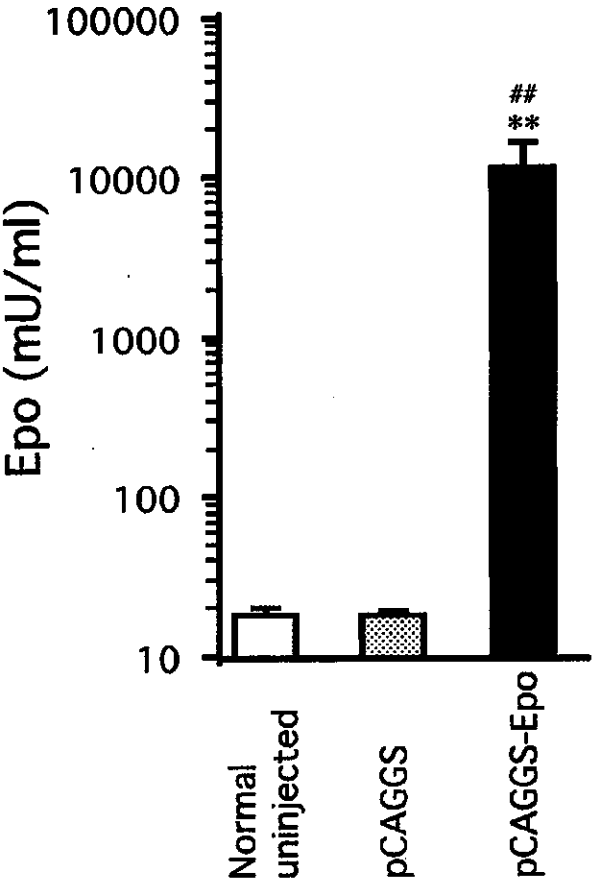

Figure 8. Serum Epo levels after pCAGGS-Epo transfer via the tail vein injection in mice. Mice were injected with 100 μg of pCAGGS-Epo ($n=5$) or pCAGGS ($n=5$) in a volume of 2.5 ml of Ringer's solution through a 27-gauge needle connected to a 2.5-ml capacity syringe into the tail vein within 5 s. Serum Epo was measured 1 week after naked DNA injection. The serum Epo levels of normal uninjected mice ($n=5$) served as the preinjection Epo levels. **, $P<0.01$ for comparisons between pCAGGS-Epo and normal uninjected mice. ##, $P<0.01$ for comparisons between pCAGGS-Epo and pCAGGS mice

three groups: each group was injected with either 100 μg of pCAGGS-Epo (pCAGGS-Epo mice; $n=5$), 100 μg of pCAGGS (pCAGGS mice; $n=5$), or no DNA (normal uninjected mice; $n=5$). According to the optimized condition of a previous report [6], we injected naked DNA in a volume of 2.5 ml of Ringer's solution through a 27-gauge needle connected to a 2.5-ml capacity syringe (Terumo) into the tail vein within 5 s. We measured the serum Epo levels of pCAGGS-Epo or pCAGGS mice 1 week after injection. We used serum Epo levels of normal uninjected mice substitute for the preinjection Epo levels. As shown in Figure 8, the serum Epo levels of pCAGGS-Epo mice (11 600 ± 2400 mU/ml) were significantly higher than those of normal uninjected mice (18.8 ± 2.2 mU/ml, $P<0.01$), or those of pCAGGS mice (18.6 ± 1.3 mU/ml, $P<0.01$). These results clearly demonstrate that pCAGGS-Epo transfer via tail vein injection in mice as well as rats can achieve sufficient Epo expression.

Discussion

Our present study demonstrates that gene transfer into the liver via tail vein injection is easily applicable to the rat, which is more than 10 times larger than the mouse.

As with previous reports on liver-targeted gene transfer by tail vein injection in mice [5,6], in the present study the two critical parameters for successful transgene expression were the injection volume and the injection speed. The optimal injection volume (25 ml) for transgene expression was approximately 100 ml/kg of the

body weight of rats. The injection volume required to reach a maximal level of gene expression was dependent on the rat weight and was probably related to the blood volume and cardiac capacity of each rat. A ratio of injection volume to animal weight of 8–12 ml/100 g was previously shown to be required for an optimal level of transgene expression [5]. The rapid injection of the appropriate volume of the DNA solution might contribute to the protection of the plasmid from degradation caused by serum and cellular nucleases [12], because the rapid injection results in the direct exposure of the DNA molecules to the hepatocytes before the DNA is mixed with blood [5].

Recently, Zhang *et al.* [13] reported the first long-term expression (6 months) of a gene in mouse liver following tail vein injection of naked DNA (the human α_1-antitrypsin gene). Miao *et al.* [14] also demonstrated that naked DNA transfer of a high-expressing nonviral human factor IX plasmid yielded long-term (over 18 months) and therapeutic-level (0.5–2 μg/ml) gene expression of human factor IX from mouse liver following tail vein injection. We verified that a transgene delivered by the tail vein injection technique could exert physiological effects. Epo gene transfer caused erythropoiesis in a dose-dependent manner. The peak serum Epo levels following the tail vein injection of 800 μg of pCAGGS-Epo were 100-fold greater than the levels reached following the muscle-targeted gene transfer of 400 μg of pCAGGS-Epo by *in vivo* electroporation [7,8]. The serum Epo levels 12 weeks after pCAGGS-Epo transfer by tail vein injection were one-tenth of the peak serum Epo levels. The serum Epo levels at 12 weeks after pCAGGS-Epo transfer to muscle by *in vivo* electroporation were one-third of the peak serum Epo levels [8]. Thus, liver-targeted gene transfer by tail vein injection has a high efficiency of gene transfer but an accelerated decline in gene expression levels, compared with transfer into muscle with *in vivo* electroporation. The mechanism of this decline is unclear. A similar early drop-off in expression in the liver has been observed in other studies [3–6,13]. Because we did not use a foreign protein in these experiments, an immune response to the transfected gene product cannot explain the present results. The loss of the transgene or promoter inactivation might have caused the unstable expression [15].

After readministering 100 μg of pCAGGS-Epo, the peak serum Epo levels of the pCAGGS-Epo 10 μg rats were lower than one-tenth of the peak levels of the pCAGGS-Epo 100 μg rats. There was no significant difference in the levels of DNA solution volume per kg body weight: 92.4 ± 5.6 ml/kg in the readministration in the pCAGGS-Epo 10 μg rats *versus* 90.4 ± 3.5 ml/kg in the pCAGGS-Epo 100 μg rats. The lower efficiency upon readministration may have been due to the rats' growth between these two injections. The pCAGGS-Epo 10 μg rats received significantly lower doses of plasmid DNA per kg body weight than did the pCAGGS-Epo 100 μg rats: 231.1 ± 14.0 μg/kg *versus* 361.7 ± 13.9 μg/kg, respectively ($P < 0.0001$). In addition, the efficiency of the gene transfer may have been affected by the increased age of the rats at the time of the second injection. For example, the intramuscular injection of naked DNA has a higher efficiency in younger animals [16]. A similar lower efficiency of Epo expression was observed after the electroporation-mediated transfer of plasmid DNA into the muscles of older rats [8].

Similar to the results in mice [13], *lacZ* gene expression after pCAGGS-lacZ injection was seen exclusively in the liver. In a previous study in which mice were subjected to hydrodynamics-based gene transfer, approximately 40% of the cells in the liver expressed the *lacZ* gene [5]. Compared with this result, the present study demonstrated a lower percentage of *lacZ*-transfected cells (Figure 3). The difference in species (mice *versus* rats) may explain the difference in gene transfer efficiency. In our experiment, the long external tube of the SURFLO winged injection apparatus slowed the speed of the injection, because the volume of liquid that could be forced through the tube in a given time was limited. This may have produced an obstacle to maximum gene transfer efficiency.

The mechanism of gene transfer via tail vein injection may be explained by hydrostatic and osmotic pressure [17], and the hydrodynamic and anatomical flow of the injected DNA solution administered using this technique [5]. The liver sinusoid wall consists of an extremely thin endothelium. The sinusoid wall is fenestrated and has no basement membrane, and is thus highly permeable to water and large molecules. We speculate that the sinusoid wall is quite permeable to Ringer's solution and large molecules, including plasmid DNA. We believe these characteristics could account for the gene transfer into hepatocytes, and the prevention of sinusoid wall rupture as a result of the large hydrostatic pressure caused by the retrograde stream of the injected naked DNA solution.

Aberrant expression is one of the concerns of using this plasmid DNA injection technique. For example, germline transmission following the tail vein injection is a possible problem. In the present study, however, transgene-derived Epo mRNA expression was not detected in the testes by real-time PCR analysis.

Liver-specific gene transfer can be achieved by using liver-specific promoters, such as the albumin promoter [18]. In general, tissue-specific, eukaryotic promoters produce substantially less expression than do viral promoters [19]. An important feature of the hydrodynamics-based transfection by tail vein injection is that it can achieve liver-targeted gene transfer with naked DNA that is driven by strong, tissue-nonspecific, viral promoters, such as the CMV promoter [5,6,13]. The present study showed that the CAG promoter ensures extremely high levels of transgene expression in the liver.

We performed the tail vein injection technique without using any specific vectors or special devices for gene transfer. The preparation of the naked DNA solution was simple, compared with lipoplex or polyplex preparation. In agreement with previous studies in mice [5,6], transient increases in serum AST and ALT levels suggested that

slight liver damage occurred under our experimental conditions. The damage is principally caused by the large volume of Ringer's solution, given that increases in serum AST and ALT levels were seen in rats with Ringer's solution injections with or without plasmid DNA. In the present experiment, liver injury attributable to gene transfer was not apparent by histological examination of the liver of injected rats.

We also noted that the transgene-derived Epo mRNA could be detected in the heart, lungs, and kidney by quantitative real-time PCR. These findings suggest that these organs could also be targeted by hydrodynamics-based gene transfection. Interestingly, transgene expression in these organs by systemic vein injection persisted longer and was apparently more stable than that in liver, as shown in Figure 2. An insufficient hydrostatic pressure caused by the tail vein injection could explain the lower levels of transgene expression in these organs. We think it likely that direct retrograde vein injection into a targeted organ will create a sufficient hydrostatic pressure for gene transfer in these organs. In fact, we have already developed a technique for kidney-targeted naked DNA transfer by retrograde renal vein injection in rats [20].

In conclusion, this liver-targeted gene transfer method should be useful for the long-term delivery of secretory proteins to examine their biological roles in rats. It can be effectively applied to rat models of diseases for gene therapy. The technique is simple and allows extremely high-level and long-term expression, which makes it particularly appealing for potential future applications in humans.

Acknowledgements

The authors are grateful to Keiko Yamagiwa and Naofumi Imai of the Division of Clinical Nephrology and Rheumatology, Niigata University Graduate School of Medical and Dental Sciences, for technical assistance.

References

1. Hickman MA, Malone RW, Lehmann-Bruinsma K, *et al.* Gene expression following direct injection of DNA into liver. *Hum Gene Ther* 1994; 5: 1477–1483.
2. Malone RW, Hickman MA, Lehmann-Bruinsma K, *et al.* Dexamethasone enhancement of gene expression after direct hepatic DNA injection. *J Biol Chem* 1994; 269: 29903–29907.
3. Budker V, Zhang G, Knechtle S, *et al.* Naked DNA delivered intraportally expresses efficiently in hepatocytes. *Gene Ther* 1996; 3: 593–598.
4. Zhang G, Vargo D, Budker V, *et al.* Expression of naked plasmid DNA injected into the afferent and efferent vessels of rodent and dog livers. *Hum Gene Ther* 1997; 8: 1763–1772.
5. Liu F, Song Y, Liu D. Hydrodynamics-based transfection in animals by systemic administration of plasmid DNA. *Gene Ther* 1999; 6: 1258–1266.
6. Zhang G, Budker V, Wolff JA. High levels of foreign gene expression in hepatocytes after tail vein injections of naked plasmid DNA. *Hum Gene Ther* 1999; 10: 1735–1737.
7. Maruyama H, Sugawa M, Moriguchi Y, *et al.* Continuous erythropoietin delivery by muscle-targeted gene transfer using *in vivo* electroporation. *Hum Gene Ther* 2000; 11: 429–437.
8. Maruyama H, Ataka K, Gejyo F, *et al.* Long-term production of erythropoietin after electroporation-mediated transfer of plasmid DNA into the muscles of normal and uremic rats. *Gene Ther* 2001; 8: 461–468.
9. Niwa H, Yamamura K, Miyazaki J. Efficient selection for high-expression transfectants with a novel eukaryotic vector. *Gene* 1991; 108: 193–199.
10. Aihara H, Miyazakai J. Gene transfer into muscle by electroporation *in vivo*. *Nature Biotechnol* 1998; 16: 867–870.
11. Maruyama H, Ataka K, Higuchi N, *et al.* Skin-targeted gene transfer using in-vivo electroporation. *Gene Ther* 2001; 8: 1808–1812.
12. Kawabata K, Takakura Y, Hashida M. The fate of plasmid DNA after intravenous injection in mice: involvement of scavenger receptors in its hepatic uptake. *Pharmaceut Res* 1995; 12: 825–830.
13. Zhang G, Song YK, Liu D. Long-term expression of human alpha1-antitrypsin gene in mouse liver achieved by intravenous administration of plasmid DNA using a hydrodynamics-based procedure. *Gene Ther* 2000; 7: 1344–1349.
14. Miao CH, Thompson AR, Loeb K, *et al.* Long-term and therapeutic-level hepatic gene expression of human factor IX after naked plasmid transfer *in vivo*. *Mol Ther* 2001; 3: 947–957.
15. Herweijer H, Zhang G, Subbotin VM, *et al.* Time course of gene expression after plasmid DNA gene transfer to the liver. *J Gene Med* 2001; 3: 280–291.
16. Wells DJ, Goldspink G. Age and sex influence expression of plasmid DNA directly injected into mouse skeletal muscle. *FEBS Lett* 1992; 306: 203–205.
17. Paillard F. Naked DNA gene delivery to the liver. *Hum Gene Ther* 1997; 8: 1735–1736.
18. Koeberl DD, Bonham L, Halbert CL, *et al.* Persistent, therapeutically relevant levels of human granulocyte colony-stimulating factor in mice after systemic delivery of adeno-associated virus vectors. *Hum Gene Ther* 1999; 10: 2133–2140.
19. Wells DJ. Intramuscular injection of plasmid DNA. *Mol Cell Biol Hum Dis Ser* 1995; 5: 83–103.
20. Maruyama H, Higuchi N, Nishikawa Y, *et al.* Kidney-targeted naked DNA transfer by retrograde renal vein injection in rats. *Hum Gene Ther* 2002; 13: 455–468.

脳と発達 2003：35；159—164

＝症例報告＝

早期より整形外科的問題を呈したメロシン陽性型先天性筋ジストロフィー

—Ullrich病との関連を含めて—

張 尚美[1] 石川 達也[1] 埜中 征哉[3]
塚本 京子[1] 斎藤万里子[1] 坂 京子[1]
和田 郁雄[2] 杉江 和馬[3] 西野 一三[3]

要旨 乳児期早期より整形外科的問題を呈したメロシン陽性型先天性筋ジストロフィー（congenital muscular dystrophy, CMD）3例の孤発例を報告した．いずれも筋生検にてメロシン陽性型CMDと診断された．症例1は13カ月時両側先天性股関節脱臼の診断を受けた．症例2は新生児期より斜頸，両側股関節拘縮が認められた．症例3は1カ月時左先天性股関節脱臼の診断を受け，コラーゲンVIの免疫組織化学染色で間質が染色されず，臨床的にはUllrich病に類似の病態であると考えられた．メロシン陽性型CMDは欠損型と異なって多因性の疾患群と考えられるのでUllrich病との関連も含めて症例の集積が必要であろう．

見出し語 メロシン，先天性筋ジストロフィー，斜頸，先天性股関節脱臼，Ullrich病

はじめに

先天性筋ジストロフィー（congenital muscular dystrophy, CMD）は福山型と非福山型に二大別され，非福山型はさらにメロシン（ラミニンα2鎖）欠損型とメロシン陽性型に分けられる．そのほか臨床的特徴によりいくつかの型が知られている．CMDは骨格筋の問題だけではなく，福山型CMDでは中枢神経障害が必発し四肢の関節拘縮が早期からみられるのが特徴的であり，メロシン欠損型CMDではCT/MRIで白質ジストロフィー様変化がみられる[1]．またCMDの一型であるUllrich病では，乳児期早期からの近位関節の拘縮と遠位関節の過伸展を特徴とする[2][3]．遺伝子変異が判明している福山型[4]，メロシン欠損型[5]およびUllrich病[6][7]に比べ，メロシン陽性型CMDは遺伝的に不均一で症例間による臨床像，病理像の差が大きい[1]．

今回我々はフロッピー・インファントで早期より先天性股関節脱臼，斜頸が認められたメロシン陽性型CMDの孤発例を3例経験し，1例ではUllrich病にみられるコラーゲンVIの完全欠損をみたので報告する．

I 症 例

症例1 14歳，女児，1988年3月生．

初診時（15カ月）主訴 筋緊張低下，運動発達遅滞．

家族歴 健康な姉が一人いる．血族結婚なし，神経・筋疾患なし．

[1]名古屋市立大学大学院医学研究科先天異常・新生児・小児医学分野
[2]同 筋・骨格系医学分野
[3]国立精神・神経センター神経研究所

連絡先 〒467-8601 名古屋市瑞穂区瑞穂町字川澄1 名古屋市立大学大学院医学研究科先天異常・新生児・小児医学分野（張 尚美）
E-mail:sangmi@u01.gate01.com

（受付日：2002. 2. 15, 受理日：2002. 9. 9）

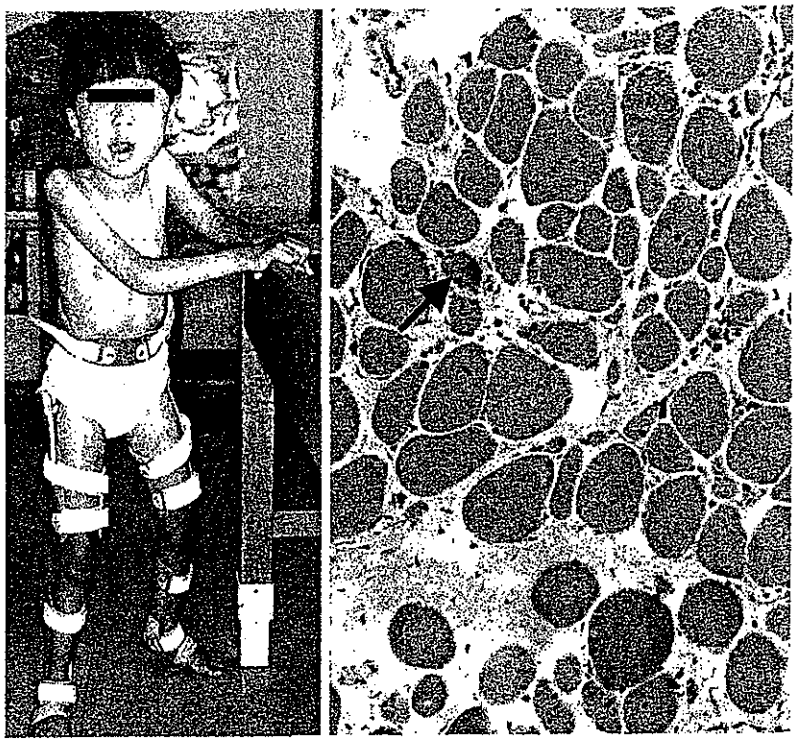

A B

図1 症例1
A:6歳時の全身像．独歩可能であった．
B:筋生検組織像．筋線維の著明な大小不同，中心核線維の増加，間質結合織の増加を認める．再生線維（矢印）も散在し，壊死・再生のプロセスがあることがわかる．
H & E染色，×500倍．

出生前・周生期歴 胎動が少なかった．前回分娩が帝王切開であったため，帝王切開で出生，骨盤位であった．在胎38週3日，2,765 gで出生した．

現病歴 乳児期早期より，フロッピー・インファントとして他院で経過観察中であった．13カ月時，側彎の評価のため行われたX線検査で，側彎はなかったが偶然両側先天性股関節脱臼が認められ，当院整形外科に紹介，筋緊張低下，運動発達遅滞が認められるため，15カ月時当科初診となった．

発達歴 定頸4カ月，座位6～7カ月，つかまり立ち24カ月，つたい歩き3歳2カ月，独歩4歳（装具使用），6歳（装具なし），あやし笑い3～4カ月，始語7カ月，二語文18カ月～24カ月と運動面での遅れがあった．

初診時現症 身長74.7 cm，体重7.1 kg，頭囲43.3 cmと正常であった．下肢装具装着中であった．全身筋緊張低下，四肢および躯幹の全般性の筋力低下を認めた．顔面筋罹患はなかった．指，手，肘，足の各関節可動域が増大していた．関節拘縮は認められなかった．膝蓋腱反射（PTR）は正常，アキレス腱反射（ATR）は消失していた．両側外反扁平足，腫骨部の突出，高口蓋を認めた．

初診時検査所見 一般生化学検査ではクレアチンキナーゼ（CK）値は215 U/l（基準値10～180）と軽度上昇していた．

経 過 先天性股関節脱臼は通常の保存的治療では改善がみられず，5歳8カ月時左側の手術が行われた．その際，左大腿直筋で筋生検を施行，筋線維の大小不同，壊死・再生結合織の増生があり（図1B）CMDと診断した．後日，メロシン染色陽性にてメロシン陽性型と診断された．コラーゲンⅥの免疫組織化学染色では間質は正常の免疫反応を示したが基底膜と思われる部位の染色性が低下していた．CK値はその後徐々に低下し11歳時には148 U/lと基準値内であった．IQはWISC-Rで，6歳時のFIQ 61（VIQ 73, PIQ 55），10歳時のFIQ 47（VIQ 50, PIQ 52）と低下していた．7歳時の頭部MRIは正常であった．11歳頃より運動面での退行がみられるようになり，筋CTでは全身の筋の著明な萎縮とCT値の低下を認めた．12歳5カ月時には独歩ができなくなり，上肢近位筋は徒手筋力テストで3以下となった．眼科的には問題はなかった．

症例2 6歳，男児，1996年7月生．

初診時（10カ月）主訴 斜頸，運動発達遅滞．

家族歴 同胞なし．血族結婚なし．神経・筋疾患なし．

とが困難であった．3歳0カ月時に施行した全身の筋CT（図3）では，同年齢でのDuchenne型およびBecker型筋ジストロフィー患児と比べてCT値が低かったため[8]，CMDを強く疑い，3歳2カ月時に右上腕二頭筋で筋生検を行った．筋線維の中等度の大小不同，軽度の壊死・再生プロセス，結合織の増生を認め，ジストロフィン染色陽性，メロシン染色陽性で，メロシン陽性型CMDと診断した．コラーゲンVIの免疫組織化学染色の結果は症例1と同じく間質は正常とほぼ同様に染色された．股関節拘縮は3歳より左股関節亜脱臼を伴い，現在整形外科，リハビリ科で経過観察中であるが，手術的治療についても考慮されている．CK値は徐々に低下し，3歳4カ月時には196 U/lと基準値内，アルドラーゼも41 ng/mlと基準値内，ミオグロビンは7.8 U/lとわずかに基準値を超えていたが，この頃より軽度の腰帯筋の筋力低下が出現した．4歳4カ月時のIQ 77，5歳9カ月時のIQ 86（ともに田研田中Binet）で教示理解がやや悪かった．4歳11カ月時に行った頭部MRIは正常，眼科的にも異常所見は認められなかった．

症例3　2歳，女児，1999年11月生．

初診時（19カ月）主訴　筋緊張低下，運動発達遅滞．

家族歴　同胞なし．血族結婚なし，神経・筋疾患なし．

出生前・周生期歴　特に問題なかった．自然分娩，頭位で在胎40週4日，2,532 gで出生した．

現病歴　1カ月健診で左先天性股関節脱臼が発見され，他院整形外科で治療中であった．4カ月健診時に筋緊張低下を指摘され，他院で精査，頭部CT，頭部MRI，眼科的には異常なかった．股関節脱臼に対しては保存的に治療が行われ，17カ月時に装具を外したが，運動発達の進展がみられないため，19カ月時当科に紹介となった．

発達歴　定頸5～6カ月，座位18カ月，独歩23カ月，始語9カ月，二語文23カ月と運動面の遅れがあった．

初診時現症　身長81.1 cm，体重8.4 kg，頭囲44.8 cmと正常であった．全身筋緊張低下を認めた．筋力低下ははっきりせず，顔面筋罹患はなかった．指，手，肘，趾，足の関節可動域が増大し，腫骨部の突出を認めた．関節拘縮はなかった．PTR，ATRは正常で高口蓋はなかった．

初診時検査所見　一般生化学検査でCK 343 U/lと軽度上昇していた．

筋病理所見　20カ月時，上腕二頭筋で筋生検を施行，筋線維の中～高度の大小不同，軽度の壊死・再生プロセス，軽度の結合織の増生を認め，ジストロフィン染色陽性，メロシン染色陽性で，メロシン陽性型CMDと診断した．コラーゲンVIの免疫組織化学染色では筋線維の基底膜と間質でコラーゲンVIは完全に欠損していた．

II 考　察

非福山型CMDはメロシン欠損型とメロシン陽性型に分けられる．そのほか臨床的特徴によりいくつかの型が知られている．欧米では，メロシン欠損型とメロシン陽性型の頻度はほぼ1:1であるが，日本ではメロシン欠損型は稀で，ほとんどがメロシン陽性型である[1]．メロシン欠損型は，遺伝子座が6q2にある劣性遺伝病で[5]，中枢神経症状はないものの脳CT/MRIで白質ジストロフィー様変化がみられ歩行獲得例は少ない．一方，メロシン陽性型は遺伝子変異が未だ不明で，症例間による臨床像，病理像の差が大きい．しかし全体的にみると軽症で90%は歩行を獲得する[1]．本症例のうち1例は知的に問題があったが福山型CMDのような重症ではなく，また脳CT/MRIでも異常がなかった．血清CK値の上昇も軽度で筋生検でも福山型CMDのような強い線維化はみられなかった．以上より福山型CMDは臨床的，病理学的に否定され，メロシン陽性型CMDと診断された．メロシン陽性型CMDは筋ジストロフィーといっても血清CK値は正常ないし軽度上昇にとどまることが多い．これは壊死・再生のプロセスが軽く緩徐進行性のためと考えられている[9]．図1Bでは壊死線維が示されているが，これは広い範囲の中でごくわずかにみられたものを示している．程度が軽いので必ずしも血清CK値の上昇と結びつかないのであろう．

CMDでは，関節拘縮をはじめ尖足，側彎などさまざまな整形外科的問題をしばしば伴う[10]．表1にメロシン陽性型CMD症例をまとめた報告を，整形外科的問題を中心に示した．Philpotらは13例のメロシン陽性型CMD患者のうち，2例で先天性に関節拘縮が認められ，そのうち1例で先天性股関節脱臼があったと報告している[11]．またKobayashiらの

本医事新報社, 1999:57-68.
2) Ullrich O. Kongenitale, atonisch-sklerotische Muskeldystrophie, ein weiterer Typus der heredodegenerativen Erkrankungen des neuromuskularen Systems. *Zschr Ges Neurol Psychiatr* 1930;**126**:171-201.
3) Nonaka I, Une Y, Ishihara T, Miyoshino S, Nakashima T, Sugita H. A clinical and histological study of Ullrich's disease (congenital atonic-sclerotic muscular dystrophy). *Neuropediatrics* 1981;**12**:197-208.
4) Toda T, Segawa M, Nomura Y, et al. Localization of a gene for Fukuyama type congenital muscular dystrophy to chromosome 9q31-33. *Nat Genet* 1993;**5**:283-6.
5) Hillaire D, Leclerc A, Faure S, et al. Localization of merosin-negative congenital muscular dystrophy to chromosome 6q2 by homozygosity mapping. *Hum Mol Genet* 1994;**9**:1657-61.
6) Higuchi I, Shiraishi T, Hashiguchi T, et al. Frameshift mutation in the collagen VI gene causes Ullrich's disease. *Ann Neurol* 2001;**50**:261-5.
7) Vanegas O C, Bertini E, Zhang R-Z, et al. Ullrich scleroatonic muscular dystrophy is caused by recessive mutations in collagen type VI. *Proc Natl Acad Sci USA* 2001;**98**:7516-21.
8) Arai Y, Osawa M, Fukuyama Y. Muscle CT scans in preclinical cases of Duchenne and Becker muscular dystrophy. *Brain Dev* 1995;**17**:95-103.
9) Kobayashi O, Hayashi Y, Arahata K, Ozawa E, Nonaka I. Congenital muscular dystrophy: clinical and pathologic study of 50 patients with the classical (occidental) merosin-positive form. *Neurology* 1996;**46**:815-8.
10) Jones R, Kahn R, Hughes S, Dubowitz V. Congenital muscular dystrophy: the importance of early diagnosis and orthopaedic management in the long-term prognosis. *J Bone Joint Surg* 1979;**61-B**:13-7.
11) Philpot J, Sewry C, Pennock J, Dubowitz V. Clinical phenotype in congenital muscular dystrophy: correlation with expression of merosin in skeletal muscle. *Neuromuscul Disord* 1995;**5**:301-5.
12) Talim B, Kale G, Topaloglu H, et al. Clinical and histopathological study of merosin-deficient and merosin-positive congenital muscular dystrophy. *Pediatr Dev Pathol* 2000;**3**:168-76.
13) 岩谷 力. 先天性股関節脱臼. 小児内科 1989;21:676-8.
14) Schmalbruch H, Kamieniecka Z, Fuglsang-Frederiksen A, Trojaborg W. Benign congenital muscular dystrophy with autosomal dominant heredity: problems of classification. *J Neurol* 1987;**234**:146-51.
15) 穐山富太郎. 筋性斜頸. 小児内科 1996;28:975-8.

Merosin-Positive Congenital Muscular Dystrophy with Early Orthopaedic Problems in Relation to Ullrich's Disease

Sangmi Chang, MD, Tatsuya Ishikawa, MD, Ikuya Nonaka, MD,
Haruko Tsukamoto, MD, Mariko Saito, MD, Kyoko Ban, MD,
Ikuo Wada, MD, Kazuma Sugie, MD and Ichizo Nishino, MD

Departments of Pediatrics, Neonatology and Congenital Disorders (SC, TI, HT, MS, KB) and Musculoskeletal Medicine (IW), Nagoya City University, Graduate School of Medical Sciences, Nagoya; National Center Hospital for Mental, Nervous and Muscular Disorders, National Center of Neurology and Psychiatry, Kodaira, Tokyo (IN, KS, INi)

We report three patients with sporadic merosin-positive congenital muscular dystrophy (CMD) with torticollis and/or developmental dislocation of the hip in early childhood. Diagnosis of merosin-positive CMD was based on their clinical and dystrophic muscle biopsy findings. At the age 13 months, patient 1 was found to have developmental dislocation of both hips; which was surgically treated at 5 years. Patient 2 had severe torticollis and contracture of both hip joints which had been present since the neonatal period, and underwent repair of the torticollis at 2 years. Patient 3 was found to have developmental dislocation of the left hip at one month of age. Although she had generalized muscle hypotonia she learned to walk at 23 months. She had no facial muscle involvement nor contracture of joints, but had hyperlaxity of distal joints. Her muscle biopsy showed complete collagen VI deficiency immunohistochemically. In contrast to merosin-deficient CMD, merosin-positive CMD appears to be a group of heterogeneous diseases. Since collagen VI was reported to be defective in Ullrich's disease, patient 3 may be diagnosed as having Ullrich's disease but had no typical clinical characteristics of the disease. Further study is needed to identify the pathogenetic mechanism of congenital muscular dystrophy with early joint abnormalities to determine whether there is a primary abnormality of the connective tissue including collagen VI.

No To Hattatsu 2003;35:159-64

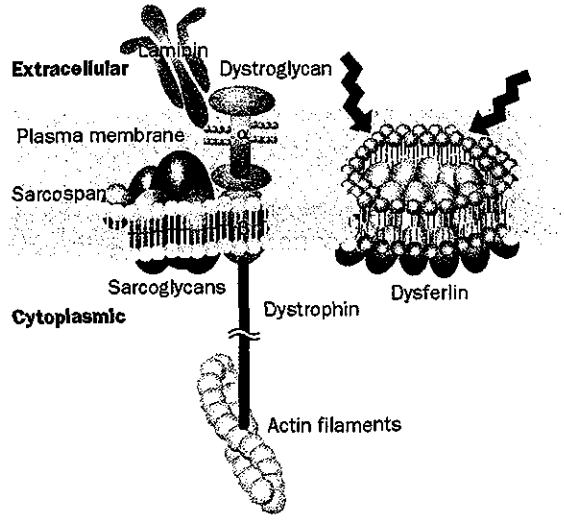

Dysferlin patch at site of disrupted membrane
Dysferlin accumulates and seals small defect in muscle membrane, while dystrophin-glycoprotein complex links extracellular basal lamina and subsarcolemmal cytoskeleton and is involved in sarcolemmal stability.

Membrane-repair machinery is thought to be involved in Ca^{2+}-dependent exocytosis of lysosomes, which are mainly predocked at the plasma membrane in non-secretory cells.[4] For example, injury-induced lysosomal exocytosis and plasma-membrane resealing in skin fibroblasts are regulated by lysosomal synaptotagmin.[5] Synaptotagmins are integral membrane proteins with two Ca^{2+}-binding C2 domains and a transmembrane domain, and are thought to serve as Ca^{2+} sensors in vesicular trafficking, exocytosis, and neurotransmitter release. Dysferlin also contains six putative C2 domains; the first C2 domain binds phospholipids, which is Ca^{2+}-dependent.[6] Because of structural similarity with synaptotagmins, dysferlin may have a similar function as a Ca^{2+} sensor, to facilitate vesicle fusion and seal disrupted skeletal-muscle membrane. Dysferlin is the first molecule to be discovered that is possibly involved in the membrane-repair machinery in skeletal muscle. Identification of other molecules associated with this machinery will help in the discovery of potential candidate genes for other muscular disorders with unknown cause.

Dysferlin can interact with caveolin-3,[7] another sarcolemmal protein that is important in the formation of caveolae, and mutations of this gene cause the dominantly inherited limb-girdle muscular dystrophy type 1C. Interestingly, abnormal cytoplasmic accumulation of dysferlin was observed in muscle from a patient with this disorder.[7] Dysferlin also accumulates in other muscular dystrophies and within the tubular aggregates, which are derived from sarcoplasmic reticulum and are especially found in various myopathies with disturbed intrasarcoplasmic Ca^{2+} homoeostasis.[8-10] These observations suggest an additional role for dysferlin in the muscle cell. Further investigations of vesicular trafficking, accumulation, and the fusion process with the plasma membrane will help to clarify the mechanisms of muscular dystrophy.

I thank Chiharu Yoshioka in my institute for drawing the figure.
I have no conflict of interest to declare.

Yukiko K Hayashi
Department of Neuromuscular Research, National Institute of Neuroscience, National Center of Neurology and Psychiatry, Kodaira, Tokyo, 187-8502, Japan
(e-mail: hayasi_y @ncnp.go.jp)

1 Cohn RD, Campbell KP. Molecular basis of muscular dystrophies. *Muscle Nerve* 2000; **23**: 1456–71.
2 Bansal D, Miyake K, Vogel SS, et al. Defective membrane repair in dysferlin-deficient muscular dystrophy. *Nature* 2003; **423**: 168–72.
3 Selcen D, Stilling G, Engel AG. The earliest pathologic alterations in dysferlinopathy. *Neurology* 2001; **56**: 1472–81.
4 Jaiswal JK, Andrews NW, Simon SM. Membrane proximal lysosomes are the major vesicles responsible for calcium-dependent exocytosis in nonsecretory cells. *J Cell Biol* 2002; **159**: 625–35.
5 Reddy A, Caler EV, Andrews NW. Plasma membrane repair is mediated by Ca(2+)-regulated exocytosis of lysosomes. *Cell* 2001; **106**: 157–69.
6 Davis DB, Doherty KR, Delmonte AJ, McNally EM. Calcium-sensitive phospholipid binding properties of normal and mutant ferlin C2 domains. *J Biol Chem* 2002; **277**: 22883–88.
7 Matsuda C, Hayashi YK, Ogawa M, et al. The sarcolemmal proteins dysferlin and caveolin-3 interact in skeletal muscle. *Hum Mol Genet* 2001; **10**: 1761–66.
8 Piccolo F, Moore SA, Ford GC, Campbell KP. Intracellular accumulation and reduced sarcolemmal expression of dysferlin in limb-girdle muscular dystrophies. *Ann Neurol* 2000; **48**: 902–12.
9 Tagawa K, Ogawa M, Kawabe K, et al. Protein and gene analyses of dysferlinopathy in a large group of Japanese muscular dystrophy patients. *J Neurol Sci* 2003; **211**: 23–28.
10 Ikezoe K, Furuya H, Ohyagi Y, et al. Dysferlin expression in tubular aggregates: their possible relationship to endoplasmic reticulum stress. *Acta Neuropathol (Berl)* 2003; **105**: 603–09.

Intervention research for suicidal behaviour

The Declaration of Helsinki states that: "The benefits, risks, burdens and effectiveness of a new method should be tested against those of the best . . . methods. This does not exclude the use of placebo, or no treatment, in studies where no proven prophylactic, diagnostic or therapeutic method exists." Nowhere is the lack of proven therapeutic methods greater than in the prevention of suicidal behaviour. Since suicide is the third leading cause of death in those under age 44,[1] the lack of randomised controlled trials that examine suicide prevention is remarkable. Reasons for such a dearth of intervention research include: a propensity for conceptualising suicidal behaviour as a general symptom of psychiatric conditions, such as schizophrenia, rather than as a specifically targetable outcome; medicolegal concerns about doing research with individuals who exhibit self-destructive behaviours;[2] and the ethical and scientific challenges of maintaining safety for participants in such studies.[3] The ethical dilemmas of the best design are thorny, including those posed by the use of placebo to minimise the occurrence of type II statistical errors arising from failed trials of efficacy rather than using treatment-as-usual interventions as comparators that putatively expose subjects to less risk.

One strategy to circumvent these problems is to examine the effects of therapeutic interventions on suicidal behaviour in analysis or meta-analyses of data developed to assess the general efficacy of pharmacotherapy on conditions such as major affective disorders or psychotic disorders. This approach compensates for the low base rate of suicidal acts, because a large number of patients are included. Indeed most controlled studies reporting pharmacological effects on suicidal behaviour have used this approach.[4-8]

Using a meta-analytic approach, Jitschak Storosum and colleagues[9] recently examined suicide attempts and completions in participants in randomised trials of atypical antipsychotics submitted to the Medical Evaluation Board in the Netherlands for approval of an indication in schizophrenia. These investigators surveyed 31 studies done between 1992 and 2002 involving 7152 patients, 1888 of whom were on placebo. At least 3759 participants were enrolled in studies that explicitly excluded suicidal patients. There was no difference in the rates of suicidal acts in those on active drug compared with those on placebo.

Human Molecular Genetics, 2003, Vol. 12, No. 22 **2895–2907**
DOI: 10.1093/hmg/ddg327

Expression profiling of FSHD muscle supports a defect in specific stages of myogenic differentiation

Sara T. Winokur[1,*], Yi-Wen Chen[2], Peter S. Masny[1], Jorge H. Martin[1], Jeffrey T. Ehmsen[1,†], Stephen J. Tapscott[3], Silvere M. van der Maarel[4], Yukiko Hayashi[5] and Kevin M. Flanigan[6]

[1]Department of Biological Chemistry, University of California, Irvine, CA, USA, [2]Children's National Medical Center, Washington, DC, USA, [3]Fred Hutchinson Cancer Research Center, Seattle, WA, USA, [4]Leiden University Medical Center, The Netherlands, [5]National Institute for Neuroscience, Tokyo, Japan and [6]Eccles Institute of Genetics, University of Utah, Salt Lake City, UT, USA

Received June 9, 2003; Revised and Accepted September 18, 2003

The neuromuscular disorder facioscapulohumeral muscular dystrophy (FSHD) results from integral deletions of the subtelomeric repeat D4Z4 on chromosome 4q. A disruption of chromatin structure affecting gene expression is thought to underlie the pathophysiology. The global gene expression profiling of mature muscle tissue presented here provides the first insight into an FSHD-specific defect in myogenic differentiation. FSHD expression profiles generated by oligonucleotide microarrays were compared with those from normal muscle as well as other types of muscular dystrophies (DMD, aSGD) in order to determine FSHD-specific changes. In addition, matched biopsies (affected and unaffected muscle) from individuals with FSHD served to monitor expression changes during the progression of the disease as well as to diminish non-specific changes resulting from individual variability. Among genes altered in an FSHD-specific and highly significant manner, many are involved in myogenic differentiation and suggest a partial block in the normal differentiation program. Indeed, many of the transcripts affected in FSHD represent direct targets of the transcription factor MyoD. Additional mis-expressed genes confirm a diminished capacity to buffer oxidative stress, as demonstrated in FSHD myoblasts. This enhanced vulnerability of proliferative stage myoblasts to reactive oxygen species is also disease-specific, further implicating a defect in FSHD muscle satellite cells. Importantly, none of the genes localizing to the FSHD region at 4q35 were found to exhibit a significantly altered pattern of expression in FSHD muscle. This finding was corroborated by expression analysis of FSHD muscle using a custom cDNA microarray containing 51 genes and ESTs from the 4q35 region. Disruptions in FSHD myogenesis and oxidative capacity may therefore not arise from a position effect mechanism as has been previously suggested, but rather from a global effect on gene regulation. Improper nuclear localization of 4qter is discussed as an alternative model for FSHD gene regulation and pathogenesis.

INTRODUCTION

Facioscapulohumeral muscular dystrophy (FSHD) is a neuromuscular disorder involving a characteristic pattern of muscles from which it derives its name (1,2). Facial weakness is frequently the earliest sign of the disease and is almost invariably present. Progression to shoulder girdle musculature often prompts the *initial clinical* evaluation. Asymmetric involvement of affected musculature is highly characteristic of FSHD, with the biceps often displaying considerable weakness, while there is a relative sparing of the deltoids. The pectoralis may be altogether absent. The basis of this asymmetry and the unique pattern of affected musculature are unknown. Extra-muscular manifestations of FSHD may include

*To whom correspondence should be addressed at: Department of Biological Chemistry, 202 Sprague Hall, University of California, Irvine, CA 92697, USA. Tel: +1 9498242750; Fax: +1 9498249547; Email: stwinoku@uci.edu
†Present address:
Johns Hopkins University School of Medicine, Baltimore, MD, USA.

sensorineural hearing loss and retinal telangiectasias, with epilepsy and mental retardation in the most severe cases (3,4). Inflammation of muscle can be a prominent histologic feature (5).

FSHD is inherited as an autosomal dominant trait, although as many as 10–30% of cases have no family history and are the result of *de novo* mutations (6,7). Age of onset typically is in the second decade of life, with nearly complete penetrance (95%) by age 20 (8). The molecular rearrangement associated with clinical development of FSHD is a deletion within a large polymorphic *Eco*RI fragment located in the subtelomeric region of the long arm of chromosome 4 (9). A 'short' *Eco*RI fragment (<38 kb) containing the probe locus p13E11 segregates with FSHD, while the size of this polymorphic locus in the normal population ranges between 38 and 300 kb. The FSHD associated DNA rearrangement is due to deletions of integral copies of a 3.3 kb tandem repeat unit termed D4Z4 contained within this *Eco*RI fragment (10). Fine mapping of this region reveals that the 4q subtelomere is mainly characterized by this large polymorphic repeat array (D4Z4) located ~25 kb proximal to the telomeric TTAGGG repeat (11–13). D4Z4 contains internal LSau and 68 bp Sau3A repeats as well as a putative open reading frame encoding two homeodomain sequences (*DUX4*) (14). However, despite intense efforts in many laboratories over the past decade, no protein coding transcripts have been identified from the D4Z4 repeat sequence (1). All characterized genes in this region map proximal to the 3.3 kb repeats (12).

Thus, FSHD results from a highly unusual mechanism in which the mutation does not reside within the gene(s) responsible for the disease. The position effect hypothesis has been invoked to explain the relationship of D4Z4 repeat deletions and the onset of FSHD (15,16). The D4Z4 repeat has several characteristics of heterochromatin, the highly condensed chromosomal structure often responsible for gene silencing (11,13,15,17–20). Although direct evidence of D4Z4 heterochromatization is lacking, the position effect hypothesis proposes that deletions of D4Z4 allow for a local decondensation of chromatin, with consequent de-repression of gene expression in the FSHD region. A multiprotein complex that binds to D4Z4 heterochromatin *in vivo* is proposed to negatively regulate gene expression, with D4Z4 deletions in FSHD permitting increased transcription at 4q35 (21).

A previous study seems to support the position effect hypothesis in FSHD, by claiming that several genes on 4q35 (FRG1, FGR2 and ANT1) are upregulated in FSHD muscle (21). While these results have yet to be replicated, it is worth noting that non-quantitative RT–PCR was used in this study. Recent analysis of these same transcripts using real-time quantitative RT–PCR has not detected upregulation of these genes in skeletal muscle from FSHD patients (M. Ehrlich and S. van der Maarel, personal communication). In addition, numerous other studies have not demonstrated altered gene expression at 4q35 (22,23). Thus, much skepticism exists regarding a possible position effect mechanism as the basis for FSHD.

The current study utilizes the GeneChip oligonucleotide microarray platform, a sensitive and specific means of identifying differentially expressed transcripts, to examine FSHD gene expression both at 4q35 as well as on a genome-wide scale (24). The majority of genes found to be dysregulated in FSHD are involved in myogenic differentiation and cell-cycle control. A custom cDNA microarray of all presently characterized 4q35 genes and ESTs was also generated in order to directly test the position effect hypothesis for FSHD. We report here that both oligonucleotide and cDNA microarray analysis do not reveal any evidence for increased expression of 4q35 genes in FSHD muscle. An alternate model for disease pathogenesis involving inappropriate nuclear localization of the FSHD chromosomal region is proposed to explain the genome-wide disruption of genes involved in myogenic differentiation.

RESULTS

FSHD gene expression profiles

Using the criteria described under data analysis (minimum 2-fold change and statistically significant at $P < 0.05$) in three FSHD patients, a total of 230 genes were found to be dysregulated, representing 3.5% of the transcripts arrayed on the HuFL GeneChip. In order to expand the number of transcripts queried and the statistical power of FSHD expression data, a larger set of biopsies (nine FSHD and six normal) was evaluated using a second GeneChip format (U95A). Utilizing the same significance criteria, a total of 297 genes (2.6%) were found to be dysregulated in FSHD muscle. Not surprisingly, a number of genes with altered expression in FSHD are also dysregulated in other forms of muscular dystrophy. Of 131 genes altered in Duchenne and a-sarcolglycan muscular dystrophy (25) using the identical GeneChip format, 35 (27%) are also altered in FSHD. All of the significant expression changes were determined using regularized *t*-test analysis within a Bayesian statistical framework, allowing for a robust estimate of variance (see Materials and Methods). Raw expression data, as well as statistical analyses of the data, are posted as supplementary data at www.ucihs.uci.edu/biochem/winokur under 'publications'.

Of the FSHD-specific dysregulated genes, a large number have a role in cellular proliferation and differentiation (Table 1). The common functional role of many of these genes is most evident in the overlap between HuFL and U95A data. Table 1 lists FSHD dysregulated genes that meet inclusion criteria for both sets of microarray data (2-fold change and $P < 0.05$ on both the HuFL and U95A GeneChips). For any particular gene, the presence on both of these 'significant gene' lists increases the confidence that that gene is involved in FSHD. The complete list of all significantly altered genes from both the HuFl and U95A GeneChips is found as supplementary data on the website www.ucihs.uci.edu/biochem/winokur.

More than half of the significantly altered genes in FSHD muscle are involved in cell-cycle control, proliferation and differentiation. Cysteine and glycine-rich protein 3 (CSRP3), also known as muscle LIM protein (MLP), is increased nearly 3-fold, whereas this transcript is not altered in the other types of muscular dystrophy studied. CSRP3 functions as a positive regulator of myogenesis (26). The LIM/double zinc-finger motif found in CSRP3 is present in proteins with essential functions in gene regulation, cell growth and somatic differentiation. Another gene involved in the differentiation of many cell types and upregulated in FSHD muscle is the delta-like homolog DLK1 (27). WEE1, a Cdk-inhibitory kinase

Table 1. Significantly altered genes in FSHD

Probe set		Gene description	Symbol	HuFL		U95A	
HuFL	U95A			*P*-value	Fold	*P*-value	Fold change
Differentiation and proliferation							
U49837	38444	Cysteine and glycine-rich protein 3 (muscle LIM protein)	CSRP3/MLP	6.9×10^{-7}	2.9	2.5×10^{-5}	2.4
HG1496-HT1496	32648	Delta-like homolog	DLK1	*2.2×10^{-2}*	*3.9*	3.1×10^{-5}	2.4
X01060	37324	Transferrin receptor (p90, CD71)	TFRC	*2.9×10^{-3}*	*7.4*	2.8×10^{-4}	4.2
D16532	36873	Very low density lipoprotein receptor	VLDLR	7.6×10^{-3}	2.5	3.1×10^{-4}	3.1
M16364	40863	Creatine kinase, brain	CKB	*4.0×10^{-5}*	*655.7*	4.1×10^{-3}	2.7
U35139	36073	Necdin (mouse) homolog	NDN	*1.9×10^{-3}*	*50.2*	5.4×10^{-3}	2.1
X59798	38418	Cyclin D1	CCND1	*1.4×10^{-2}*	*101.9*	6.3×10^{-3}	2.2
X62048	2033	Wee1 + (S. pombe) homolog	WEE1	*1.5×10^{-3}*	*7.6*	*4.1×10^{-2}*	*2.5*
M10942	36130	Metallothionein 1E	MT1E	1.5×10^{-2}	−2.0	3.6×10^{-5}	−2.7
X76717	39120	Metallothionein 1L	MT1L	4.3×10^{-3}	−2.5	7.0×10^{-5}	−2.6
X64177	39594	Metallothionein 1H	MT1H	1.1×10^{-3}	−2.8	1.3×10^{-4}	−3.6
X52541	789	Early growth response 1	EGR1	*4.6×10^{-2}*	*−2.8*	4.5×10^{-3}	−2.3
U47414	37723	Cyclin G2	CCNG2	*1.9×10^{-2}*	*−3.8*	5.4×10^{-3}	−2.4
M62831	36097	Immediate early protein	ETR101	*4.3×10^{-3}*	*−4.0*	3.2×10^{-2}	−2.1
Transcription factors							
M83667	1052	CCAAT/enhancer binding protein (C/EBP), delta	CEBPD	4.4×10^{-3}	−2.4	1.7×10^{-3}	−2.4
M13929	37724	v-myc avian myelocytomatosis viral oncogene homolog	MYC	3.0×10^{-3}	−2.3	*4.0×10^{-3}*	*−4.5*
Energy metabolism							
U54617	36739	Pyruvate dehydrogenase kinase, isoenzyme 4	PDK4	*9.6×10^{-3}*	*−4.3*	3.6×10^{-6}	−6.9
Extracellular matrix							
X06700	32488	Collagen, type III, alpha 1	COL3A1	5.4×10^{-6}	6.9	4.5×10^{-6}	6.7
L13923	32535	Fibrillin 1 (Marfan syndrome)	FBN1	5.5×10^{-4}	2.6	8.9×10^{-4}	2.7
L32137	40163	Cartilage oligomeric matrix protein	COMP	*1.1×10^{-2}*	*−8.3*	*3.4×10^{-2}*	*3.6*
Others and unknown							
L36033	32666	Stromal cell-derived factor 1	SDF1	9.3×10^{-3}	2.0	1.4×10^{-3}	2.2
U09770	33232	Cysteine-rich protein 1 (intestinal)	CRIP1	2.9×10^{-3}	2.2	4.2×10^{-3}	2.1
S71043	33499	SNC73 protein (SNC73)	ASPA	8.0×10^{-3}	2.6	3.0×10^{-2}	2.1
M34516	33274	Immunoglobulin lambda-like polypeptide 2	IGLL2	5.0×10^{-3}	2.3	*3.1×10^{-2}*	*9.1*
S73591	31508	Thioredoxin interacting protein	TXNIP	1.9×10^{-3}	−2.3	2.2×10^{-6}	−2.5
HG1862-HT1897	955	Calmodulin	CALM	5.9×10^{-3}	−2.0	1.6×10^{-3}	−2.1
D86640	40024	src homology three (SH3) and cysteine-rich domain	STAC	1.7×10^{-2}	−2.9	*1.4×10^{-2}*	*−4.3*

Fold changes in italics are generated from experimental groups with one or more samples with a '0' expression value. These values are thus both greater in magnitude and less accurate.

that functions in part to arrest the cell cycle (28), is elevated in FSHD. The transferrin receptor TFRC is also elevated in FSHD muscle. Transferrin is a key myoblast trophic factor, initially promoting myoblast proliferation and subsequently supporting myogenic differentiation (29). Two other genes, very low density lipoprotein receptor (VLDLR) and necdin (NDN), which play important roles in differentiation, are upregulated in FSHD muscle. VLDLR is required for neurogenesis of the cerebral cortex (30) and necdin is an imprinted gene that suppresses growth in postmitotic neurons (31).

Other genes of interest in light of FSHD pathophysiology include immunoglobulin lambda-like polypeptide 2 (IGLL2) and thioredeoxin interacting protein TXNIP (also known as vitamin D3 up-regulated protein 1, VDUP1). As FSHD muscle often has marked inflammatory infiltrates (5), identifying specific genes involved such as IGLL2 may prove valuable in dissecting the role of the immune response in this disease. TXNIP functions as an oxidative stress mediator by inhibiting activity of thioredoxin, which is a potent thiol reductase and reactive oxygen species regulator (32). TXNIP is down-regulated in FSHD muscle, a finding consistent with the enhanced vulnerability to oxidative stress seen in FSHD myoblasts (33). Interestingly, a number of metallothionein (MT) transcripts are also reduced in FSHD muscle. Metallothioneins are a group of ubiquitous low MW proteins that have functional roles in cell growth, repair and differentiation. MTs serve to protect against free radical toxicity during the differentiation of myoblasts to myotubes (34).

Independent confirmation of CSRP3/MLP and DLK1 upregulation

In order to independently verify expression changes of a small subset of genes involved in differentiation (CSPR3 and DLK1), real time RT–PCR (TaqMan) analysis was carried out (35). Owing to limiting RNA isolated from muscle biopsies used for GeneChip analysis, only a few samples and primer sets were used for confirmation. A negative control was chosen which did not demonstrate altered expression according to microarray analysis. Actinin-associated LIM protein (ALP) maps to the FSHD gene region and is not altered in FSHD (22,36). Expression levels for all transcripts were determined relative to the internal housekeeping control gene ribonucleoprotein S1 (RPNS1) (37). As Figure 1 demonstrates, both CSPR3 and